FISEVIER

Contents lists available at ScienceDirect

Quaternary Science Reviews

journal homepage: www.elsevier.com/locate/quascirev



Climatic control on magnetic mineralogy during the late MIS 6 - Early MIS 3 in Lake Chalco, central Mexico



Beatriz Ortega-Guerrero ^{a, *}, Diana Avendaño ^b, Margarita Caballero ^a, Socorro Lozano-García ^c, Erik T. Brown ^d, Alejandro Rodríguez ^b, Bernardo García ^b, Hermenegildo Barceinas ^b, Ana María Soler ^a, Albán Albarrán ^b

- ^a Universidad Nacional Autónoma de México, Instituto de Geofísica, 04150, Ciudad de México, Mexico
- ^b Universidad Nacional Autónoma de México, Posgrado en Ciencias de la Tierra, 04150, Ciudad de México, Mexico
- ^c Universidad Nacional Autónoma de México, Instituto de Geología, Ciudad de México, 04150, Mexico
- d University of Minnesota Duluth, Large Lakes Observatory and Department of Geological Sciences, Duluth, MN, 55812, USA

ARTICLE INFO

Article history: Received 23 August 2019 Received in revised form 12 December 2019 Accepted 1 January 2020 Available online 20 January 2020

Keywords: Pleistocene Interglacial(s) Paleolimnology North America Magnetic properties

ABSTRACT

Sediments from Lake Chalco in central Mexico spanning from ca. 150 to 35 ka ago provide evidence of paleoclimatic variability in the North American tropics associated with the end of Marine Isotopic Stage (MIS) 6, the transition to the last interglacial (MIS 5.5, ca. 130-115 ka ago), and part of the last glacial (MIS 5.4 to early MIS 3, 115 to 35 ka ago). We applied a multiproxy approach based on the analysis of mineral magnetism, diatom assemblages and major elements geochemistry. The reconstructed paleoenvironmental history identify the end of the globally cool MIS 6 as wetter than present, with high lake level, and a subsequent change to drier climates at the onset of the last interglacial (ca. 130 ka). Large amplitude changes in most of the analyzed parameters from ca. 130 to 74 ka are approximately coincident with MIS 5 (130-71 ka). The amplitude of these changes decreases in MIS 4 (71-57 ka) and the early part of MIS 3 (57-35 ka). We proposed that the inferred climatic oscillations follow insolation variations during MIS 6 and part of MIS 5 (150-88 ka). Low summer and spring insolation and lower seasonality inhibited evaporation and favored high lake levels. Conversely, maxima in spring and summer insolation promoted dry conditions and low lake levels. The major wet-cold glacial and dry-warm interglacial relationship found in Lake Titicaca (Bolivia) and Lake Chalco records shows the sensitivity of high altitude tropical sites to climatic variability.

© 2020 Elsevier Ltd. All rights reserved.

1. Introduction

Lacustrine sedimentary records worldwide have been analyzed as archives of past climatic conditions; however, published records beyond the last glacial maximum (>20 ka) are infrequent for the tropics of North America (e.g. Caballero et al., 1999; Ortega et al., 2002; Metcalfe et al., 2007; Israde-Alcántara et al., 2010; Caballero et al., 2019). Climatic records of the past 85 ka have been published from Lake Petén Itzá (Guatemala) (Hodell et al., 2008; Mays et al., 2017), and Lake Chalco (México) (Torres Rodríguez et al., 2015, 2018). Longer records that comprise the last interglacial (ca.

E-mail address: bortega@igeofisica.unam.mx (B. Ortega-Guerrero).

130-115 ka) are practically nonexistent so far in the North American tropics. In Central America the only record is available from El Valle (Panamá) spanning the time period between 137-98 ka (Cárdenes-Sandí et al., 2019). In central Mexico the stratigraphical and sedimentological characteristics of Lake Chalco provide some inferences of paleoclimate and paleoenvironments beyond the last interglacial (Ortega-Guerrero et al., 2017; Valero-Garcés et al., 2019). From South America, long records include the sequence from Lake Titicaca (Bolivia) which covers the last ca. 370 ka (Fritz et al., 2007), and Lake Fúquene (Colombia) for the last 280 ka (Groot et al., 2011). More studies on long lacustrine sedimentary sequences will advance our understanding of climatic variations during the last interglacial/glacial cycle. Such knowledge is relevant to establish correlations with similar events recorded at sites on the opposite hemisphere and to test their synchronicity and geographical extent. These kinds of records can also be used to

^{*} Corresponding author. Universidad Nacional Autónoma de México, Instituto de Geofísica, Ciudad Universitaria circuito exterior s/n, 04150, Ciudad de México, Mexico.

characterize the climate dynamics in the tropics, and to evaluate the response of ecosystems to similar climatic drivers, but under contrasting conditions; for example, as during interglacials without (Marine Isotopic Stage 5) and with (Marine Isotopic Stage 1) human influence.

The use of independent proxies in the interpretation of these records is recommended, in order to achieve a more comprehensible model of past environmental changes driven by climatic fluctuations. Therefore, a multiproxy approach is necessary, including a combination of techniques such as stable isotopes, elemental concentrations, biological proxies and rock magnetism analyses. Studies on environmental magnetism investigate the changes in the detrital magnetic mineral fraction and its transformation into new secondary minerals (Maher, 2007). In volcanic settings, Ti-magnetites are a common detrital fraction in lacustrine sediments (e.g. Thouveny et al., 1994). Weathering and pedogenesis processes can produce secondary minerals that can be delivered to lakes as a detrital fraction (e.g. Chen et al., 2005; Maxbauer et al., 2016a). Anoxic conditions may lead to the dissolution of Fe oxides and their transformation into sulfurs (e.g. Nowaczyk, 2011; Borruel-Abadía et al., 2015); and bacterial processes can produce secondary minerals (e.g. Lascu and Plank, 2013). The aforementioned transformations suffered by magnetic minerals depend to a great extent on climatic and environmental controls (e.g. Evans and Heller, 2003), so they are potential indicators of past climatic conditions. We present a continuous ~115 ka (150-35 ka BP) record of paleoenvironmental change inferred from rock magnetism, elemental geochemistry and synthetic results of diatom analyses from a 93 m long lacustrine sedimentary sequence collected in Lake Chalco (central México), which constitutes a unique record of most of the last interglacial/glacial cycle in the North American tropics. New insights of past climatic and environmental changes between the late MIS6 and early MIS 3 are provided through diagnostic magnetic parameters of the alteration of the primary mineralogy and the changes between freshwater and saline diatom taxa. This study differs from previous from Lake Chalco as it constitutes the longest continuous published record of past climatic and environmental conditions based on any proxy.

2. Geological setting and climate

Lake Chalco is an intervolcanic basin located at the centraleastern sector of the Trans Mexican Volcanic Belt (TMVB), a transversal continental arc that resulted from the subduction of the Cocos Plate beneath the North American Plate (Ferrari et al., 2012) (Fig. 1). The Chalco sub-basin occupies the southeastern part of the Basin of Mexico (19° 15' N, 98° 58' W, 2230 m asl), at the southern edge of Mexico City metropolitan area. Even if in past times there was an extensive lake, it is now reduced to a shallow marsh (<3 m depth), that occupies an area of <6 km². The rocks in the catchment are entirely composed of volcanic deposits, mostly ranging from basalts to andesites in composition, which include scoria and ash cones, shield volcanoes and associated lava flows, fisural lava flows, domes, maars and stratovolcanoes, among them two of the highest summits in Mexico, the Popocatépetl (5452 m asl) and Iztaccíhuatl (5238 m asl), built since 1.8 Ma to present (Macías et al., 2012; Arce et al., 2013).

The climate is sub-tropical high altitude, with a mean precipitation of 540 mm/yr, concentrated during the summer months (late June to September) due to the northern migration of the Intertropical Convergence Zone (ITCZ) and the onset of hurricane season; occasional rainfall occurs during the winter caused by polar air outbreaks. Maximum temperatures (27–30 °C) occur during late spring and the lowest temperatures (4–7 °C) are observed during winter.

3. Materials and methods

3.1. Drilling, facies description and core correlation

The drilling details, core correlation, lithostratigraphy of the sequence and geochronology of the upper 122 m of the sedimentary sequence have been published previously (Ortega-Guerrero et al., 2017). Three cores were drilled in 2008 at different depths at the depocentre zone of former Lake Chalco. The cores span a composite section between 29 and 122.4 m depth: CHA08-IV (85-122 m), CHA08-V (29-72 m), CHA08-VI (70.8-85 and 106–122.4 m). The cores were drilled with a Shelby corer in 1.10 m sections with inner PVC tubes 1 m long and 10 cm in diameter; the remaining 10 cm were collected from the drilling shoe. Splitting of cores and initial description were carried out at the LacCore facility (University of Minnesota-Twin Cities). High-resolution color scans were acquired from each section using a DMT CoreScan digital linescan camera, and magnetic susceptibility was measured on split halves at 0.5 and 1 cm resolution using a Bartington MS2E sensor. The correlation of the cores was established from stratigraphic features, tephra markers and the magnetic susceptibility profiles.

Nineteen sedimentary facies had been previously established from component descriptions in smear slides and visual observations of the core faces for the entire sequence from the surficial sediments to 122.4 m depth (Ortega-Guerrero et al., 2017). However, for the section analyzed in this work, only fourteen facies are present and the rest occur only in the upper 29 m (Table 1). Based on their facies association, seven lithostratigraphic units that reflect the main stages of Lake Chalco evolution were defined for the entire sequence, of which correspond from unit 4 to unit 7 in the analyzed section in this work (Fig. 2).

The sedimentary facies defined were grouped into clastic, volcaniclastic, organic rich and chemical facies. The clastic facies are the most abundant in the sequence (F5 to F12); they vary from massive to faintly laminated silt with variable content of sand and clay and are composed of siliciclastic minerals. Organic components in these facies are commonly diatoms, ostracods, charophytes, phytolites and charcoal; other components are sponge spicules, testate amoebae, amorphous organic matter, unidentified Arthropoda fragments and occasionally Phacotus. The organic rich facies (F14, F15 and F17) are most commonly diatom oozes and occur less abundant as ostracod hashes. Diatom oozes form beds (<3 cm) and laminae; locally they form pairs of light/dark laminae. Ostracod hashes have a variable content of sand-size fraction clasts. The chemical facies (F18 and F19) are carbonate-rich silt beds or laminae and micritic mud. Other minor chemical components are crystals of struvite, vivianite, siderite, calcite and gypsum. Lithostratigraphic units defined from facies association were described by Ortega-Guerrero et al. (2017) and shown in Fig. 2.

3.2. Geochronology

In the upper 35 m of the master sequence, the age-depth model was constructed from fourteen ¹⁴C AMS dates obtained from pollen and ostracod concentrates, and two tephrostratigraphic ages markers (Ortega-Guerrero et al., 2017, Table 1 Supplementary Material). For the deeper part of the section beyond the ¹⁴C limit, chronology was established by dating zircons extracted from a tephra layer at a depth of 63.5 m using ²³⁰Th/U (Torres Rodríguez et al., 2015), and including a tie-point at 106 m depth where a major change in sedimentary components, structure and diatom assemblage is considered to correspond to the transition from marine isotopic stage (MIS) MIS 6 to MIS 5 (Ortega-Guerrero et al., 2017; Avendaño-Villeda et al., 2018). The age obtained in by ²³⁰Th/U dating was 76.7 ± 4.7 ka, whereas the age of the MIS6-MIS5 limit is

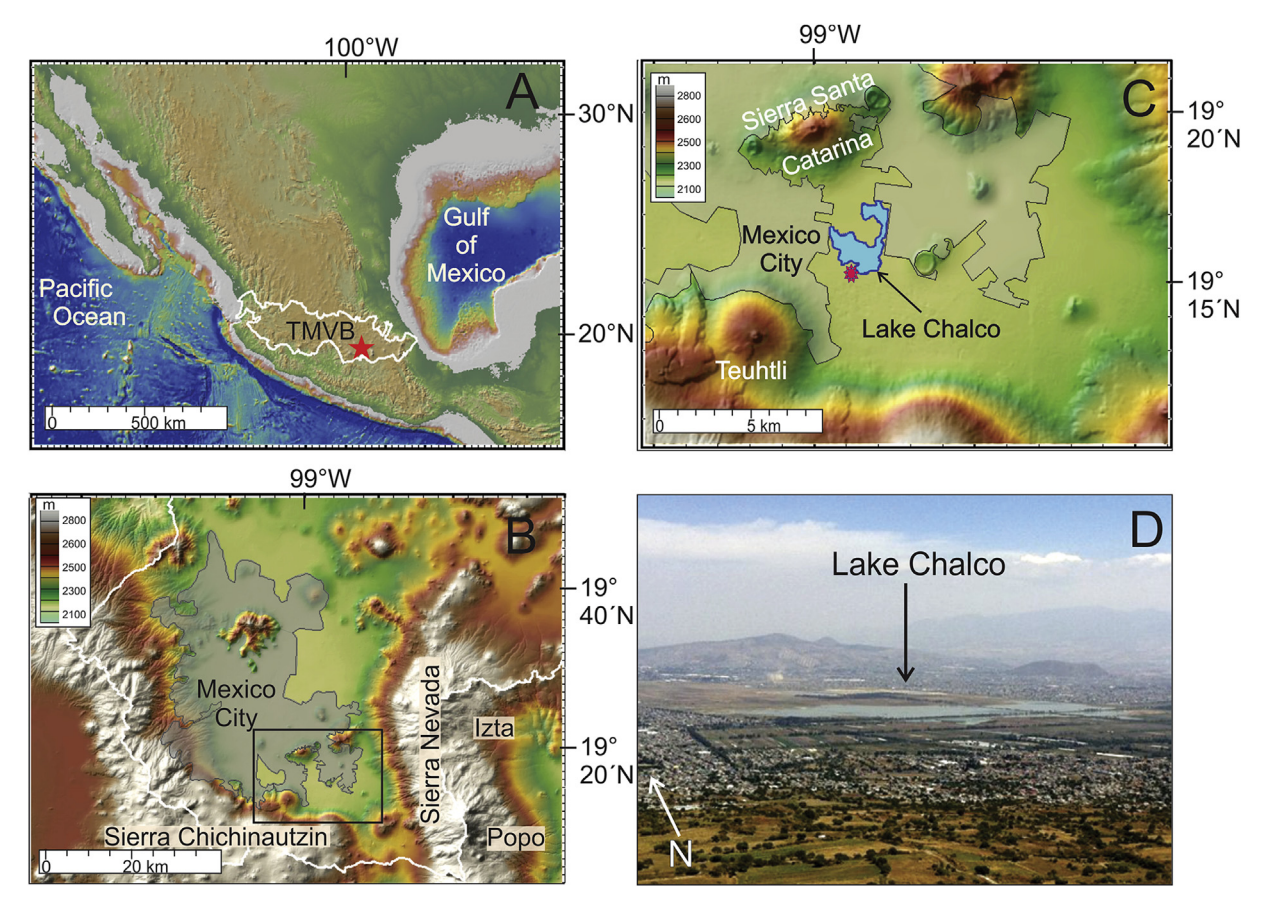


Fig. 1. Location map of Lake Chalco and drilling site. A) Extent of the Trans Mexican Volcanic Belt (TMVB) in central Mexico; red star: location of Basin of Mexico. B) Relief map showing the southern part of Basin of Mexico (white contour). Major stratovolcanoes Popocatepetl (Popo, 5605 m asl) and Iztaccihuatl (Izta, 5460 m asl) of the Sierra Nevada and location of Sierra Chichinautzin are shown. Gray shaded area correspond to the extent of Mexico City metropolitan area. The study area of figure C is outlined in black rectangle. C) Relief map of Lake Chalco and drilling sites of cores CHA08-IV, V and VI (red star). D) Lake Chalco seen from the summit of Teuhtli volcano. (For interpretation of the references to color in this figure legend, the reader is referred to the Web version of this article.)

 130 ± 3 ka, according to Lisiecki and Raymo (2005) and Lisiecki and Stern (2016). The age model for the sequence, including the 14 C dates, the 230 Th/U age and the MIS 6-MIS 5 tie point was constructed on a P-sequence deposition model (Bronk-Ramsey, 2008) generated in the online version of OxCal 4.2 (Bronk-Ramsey, 2009) using the IntCal 13 calibration curve (Reimer et al., 2013). The age of the analyzed section of the master sedimentary sequence in this work (29–122 m) was estimated between ca. 35.6 to 150 ka (Ortega-Guerrero et al., 2017) (Fig. 3).

3.3. Geochemical and rock magnetism analyses

The elemental geochemical composition was analyzed using a COX ITRAX X-Ray Fluorescence (FRX) core scanner at 1 cm resolution using a Mo-tube X-ray source set to 30 kV and a current of 20 mA, with an exposure time of 60 s. Although the XRF scanner was capable of detecting 21 elements reliably above detection limits (Al, Si, P, S, Cl, Ar, K, Ca, Ti, V, Cr, Mn, Fe, Zn, Ga, As, Se, Rb, Sr, Zr, W), only a set of elements and their ratios were used in this work (Ca, Ti, Fe, Mn).

Cores were sampled in roughly 10 cm intervals, with minor adjustments to obtain samples from all of sedimentary facies in each core. The 840 samples acquired were placed in 8 cm³ diamagnetic plastic cubes and stored in a cold room until all measurements were completed. Rock magnetic measurements carried out on the full set of samples consisted of mass-specific magnetic susceptibility (χ), the acquisition of anhysteretic

remanent magnetization (ARM), isothermal remanent magnetization (IRM) and hysteresis parameters (saturation magnetization [Ms], saturation remanent magnetization [Mr], coercivity [Bc] and coercivity of remanence [Bcr]). Magnetic susceptibility was measured at low (976 Hz) and high (hf, 15916 Hz) frequencies in a MFK1-FA (AGICO) susceptometer. Frequency-dependent susceptibility was calculated as $\kappa fd \% = [(\kappa lf - \kappa hf)/\kappa lf]^* 100$. ARM and IRM were measured in a JR6 spinner magnetometer. ARM was imparted in a peak alternating field (AF) of 100 mT in the presence of a direct current (DC) bias field of 50 μ T. The ARM susceptibility (χ_{ARM}) was obtained by normalizing the ARM by the DC biasing field. The hysteresis parameters were measured using a Princeton Measurements Corporation Micromag vibrating sample magnetometer (VSM) at room temperatures in fields up to 1 T. Saturation IRM (SIRM) was considered to be acquired in a 1 T field. IRM was measured in backfields of 100 and 300 mT after the acquisition of SIRM, and HIRM and S_{300} ratios calculated, where HIRM = 0.5 * $(SIRM + IRM_{-300 \text{ mT}})$, and $S_{300} = - (IRM_{-300}/SIRM)$.

In 46 selected samples from the representative magnetic properties, backfield remanence curves in 100 steps were measured in the VSM in order to identify the individual components that contribute to the remanence by using the MAX UnMix program (Maxbauer et al., 2016b). The temperature-dependence of susceptibility (κ -T) was measured for selected samples in a noncontrolled atmosphere from room temperature to a maximum of 700 °C using a MFK1-FA (AGICO) susceptometer.

Table 1Main sedimentological and mineralogical features, compositional parameters for the facies defined for Lake Chalco sedimentary sequence from 29 to 122.4 m depth (Ortega-Guerrero et al., 2017).

Facies	Sedimentological features	Depositional environment
Clastic	5. Olive brown sandy silt . Massive to faintly laminated and bedded. Very dark grayish brown laminae (1 cm) and beds (1–2 cm). Abundant biogenic components: diatoms (occasionally partly dissolved), charophyte particles, ostracods and charcoal. Occasional clay size calcareous particles and calcite, dolomite and gypsum crystals.	Shallow lake, minor influence of lotic systems. Perimetral facies with variable phases of vegetation growth.
	6. Very dark grayish brown to dark reddish brown sandy silt . Presence of calcareous silt. Massive strata <15 cm thick, and beds 1–3 cm. Undulating irregular contacts. Features of vertical movement of groundwater. Scarce biogenic components: ostracod, diatoms, herbaceous fragments and charcoal.	Palustrine facies. Well drained environment, lixiviation. Subaereal exposure. Slightly to moderately pedogenic processes.
	7. Dark grayish brown sandy silt. Discontinuous and wavy, parallel volcaniclastic rich sandy silt beds and silt sediments. Frequent ostracods and calcareous silt. Minor amounts of diatoms.	Low lake levels. May represent distal deposits of detrital fluxes.
	8. Grayish brown silt to sandy silt . Decimetric (10–60 cm) massive beds, with intercalations of silt beds (2–20 cm). Sharp and irregular contacts. Sand particles disseminated in beds <15 cm thick, and in irregular bands 1–2 cm thick. Abundant biogenic components: ostracods, diatoms, spicules.	· · · · · · · · · · · · · · · · · · ·
	9. Very dark grayish brown clayey silt . Massive to faintly laminated. Minor amounts of lithic sand. Presence of <i>Staurosira</i> spp. and <i>Staurosirella</i> spp. Sharp to gradual contacts.	Shallow freshwater lake with minor influence of lotic systems
	10. Dark olive brown to pale yellow clayey silt . Diffuse, wavy, parallel beds 4 –10 cm. Abundant clay size calcareous (calcite, dolomite) mud. Presence of <i>Chara</i> and charcoal. Scarce to common ostracod fragments. In general minor amounts of diatoms.	
	11. Dark olive gray clayey silt . Mottled and massive at naked eye. Centimetric to decimetric wavy bedding. Presence of clay size calcareous minerals and biogenic components: <i>Chara</i> (abundant), ostracods. Diatoms relatively less abundant partly dissolved, charcoal, phytoliths, cysts.	
	12. Dark olive gray to light gray bedded and laminated diatom rich silt. Sets of beds (2–6 cm) and laminae. Light strata are diatom ooze with scarce ostracods, detrital crystals (silicates), and calcareous mud. Dark strata are diatom rich silt. Parallel, slightly wavy strata.	Shallow alkaline-saline lake.
clastic	13. Black to gray ash layers . 74 individual medium to very fine grained mafic to felsic ash layers. Massive to bedded. Frequent ostracods and variable content of diatoms. Thicknesses of 0.5–8 cm. Lower loaded contacts are common. Vivianite occurs in some tephra layers.	sources. The basaltic to dacitic deposits are more likely form the near monogenetic ranges Chichinautzin and Santa Catarina. Dacitic to rhyolithic deposits are more likely from distal stratovolcano sources.
Organic- rich	14. Light olive brown to dark olive gray laminated diatomaceous silt and diatom ooze. Sets of light/dark laminae. Light laminae are composed of diatom ooze dominated by Stephanodiscus niagarae, S. oregonicus, Cyclotella quillensis, C. meneghiniana. Presence of spicules, charcoal, and minor amounts of vivianite and gypsum. Biogenic components are covered by calcareous microcrystals. Dark laminae are composed of calcareous algae, ostracode fragments, testate amoebae, Phacotus, and presence of diatoms: Surirella peisonis, Ephitemia and C. meneghiniana.	
	15. Grayish brown laminated diatom ooze and dark olive gray diatomaceous silt. Sets of rhythmic light/dark laminae. Light laminae are diatom ooze dominated by Stephanodiscus. niagarae and S. oregonicus. Dark laminae are silt with minor calcareous components. Abundant diatoms: S. niagarae, Fragilaria capuchina, Surirella peisonis. Presence of ostracodes and scarce Chara. Contacts are planar, parallel.	Relatively deep (few meters), stratified, cold to temperate fresh water lake. Anoxic conditions in the hypolimnion (Avendaño-Villeda et al., 2018).
	17. Ostracod hash . Commonly with sand-size fraction clasts. Color variable depending on the composition of the clast fraction. Beds 1–3 cm thick. Well preserved ostracod valves. In the facies 11 <i>Heterocypris</i> spp. and <i>Candona</i> spp. are abundant. Commonly associated to facies 3, 4, 6, 7, 9 and 10.	Shallow lake, dominant endogenic sedimentation. The well preserved ostracod shells indicate low energy environment.
Chemical	18. Dark gray to pale yellow carbonate-rich silt . Bedded (2–15 cm thick) to laminated. Silt sized particles of autochthonous carbonate (calcite, dolomite, ankerite). Frequent intercalations of diatom ooze laminae composed of <i>Cyclotella meneghiniana</i> , <i>Anomoeoneis costata</i> and <i>Campilodiscus clypeus</i> , and cm-thick sandy layers of ostracod hash.	
	19. Pale yellow micritic mud. Banded (2–5 cm thick). Calcite is dominant, followed by siderite, dolomite, and minor amounts of clay minerals. Abundant diatoms: <i>S. niagarae</i> , <i>C. clypeus</i> , <i>S. oregonicus</i> , <i>A. costata</i> , and frequent ostracods.	Relatively deep (few meters), stratified, temperate, alkaline lake. Anoxic conditions in the hypolimnion (Avendaño-Villeda et al., 2018).

3.4. Diatoms

Sediment samples for diatom analyses were collected on average every 30 cm, and cleaned using HCl, $\rm H_2O_2$ and HNO₃. Clean material was mounted in permanent slides using Naphrax, and diatom counts were undertaken at $1000\times$ using an Olympus BX50 microscope. Here we present summary results on the relative abundance of small Fragilariaceae and *Stephanodiscus* spp., which

are considered indicative of freshwater conditions, and the sum of alkaliphilous and halophilous taxa; these categories were defined according to the species ecological preferences defined by the analysis of diatom species distribution along 40 lakes in central Mexico (Caballero et al., 2019). Main halophilous taxa were Anomoeoneis costata, A. sphaerophora and Camphylodiscus clypeus; main alkaliphilous taxa were Cyclotella meneghiniana, N. amphibia and Surirella peisonis. Stephanodiscus spp includes S. niagarae which

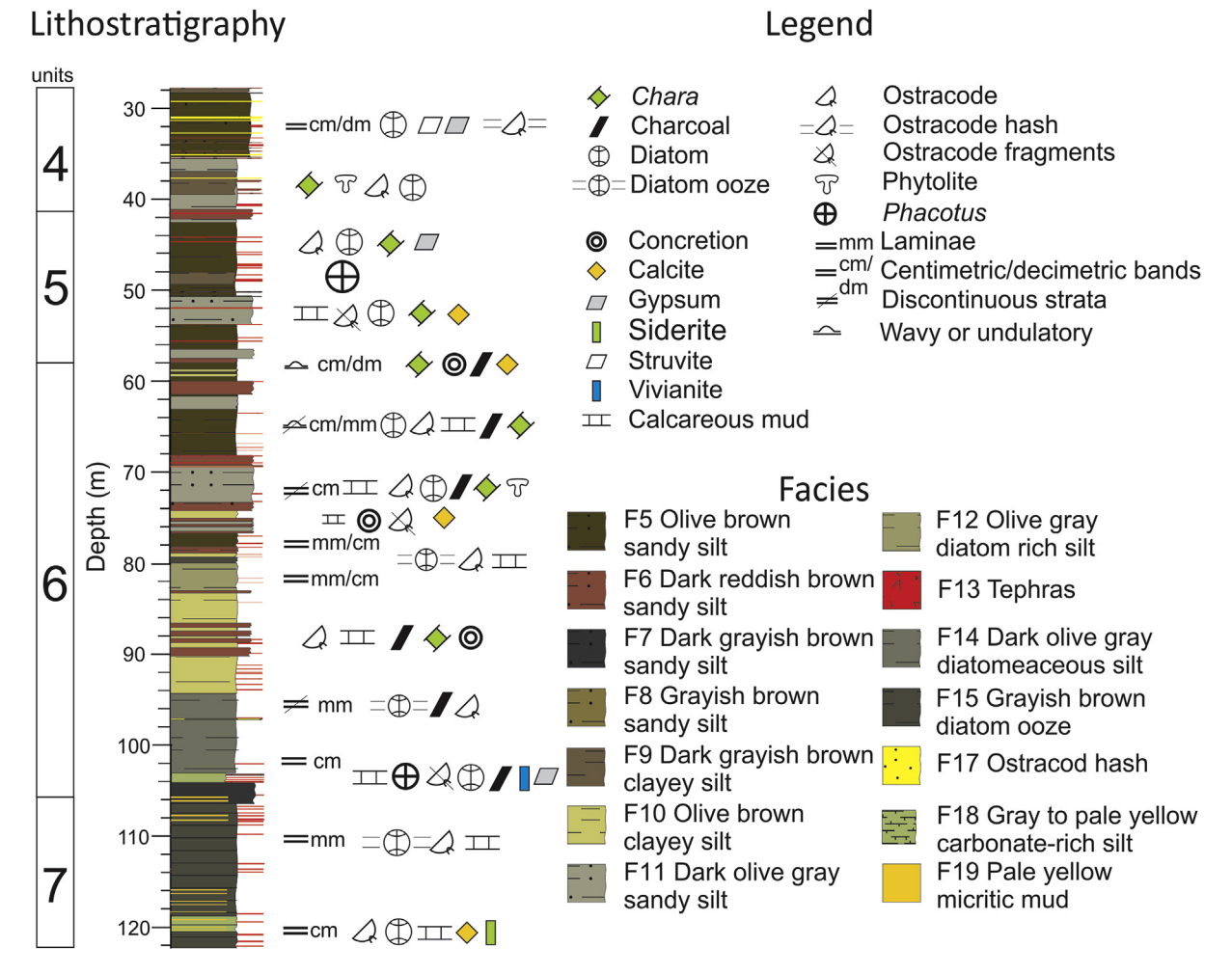


Fig. 2. Lithostratigraphy of the master sequence of cores CHA08 IV-V-VI from 29 to 122.4 m depth, showing the lithostratigraphic units 4–7 described in Ortega-Guerrero et al. (2017).

besides being indicative of freshwater conditions is also considered indicative of cooler conditions (Avendaño-Villeda et al., 2018).

4. Results

4.1. Downcore profiles

The diatoms have a distinctive distribution along the record, which mostly correlates with the lithostratigrphic units (Fig. 4). Geochemical composition and magnetic properties are strongly facies-dependent and most parameters and ratios show a good correlation with the lithostratigraphic units. Therefore, the results are described following the lithostratigraphic boundaries. The geochemical elemental ratios used are: Ca/Ti as an indicator of authigenic carbonates (e.g. Haberzettl et al., 2007); Mn/Fe as an oxidation proxy (e.g. Oliva-Urcia and Moreno, 2019); and Fe/Ti is used to identify iron diagenetic enrichment (e.g. Aufgebauer et al., 2012) (Fig. 4.).

Concentration-dependent parameters of magnetic minerals are shown in Fig. 5 and they include magnetic susceptibility (χ), χ_{ARM} , SIRM and HIRM₃₀₀. Particle-size dependent parameters include fine particle-size (SD) indicator ratio κ_{ARM}/IRM_{100} and ultrafine superparamagnetic (SP) particle-size indicator κ fd %; and coercivity-dependent HIRM₃₀₀ and S₃₀₀ ratios and parameter Bcr. They were plotted with a 5-point running average (black lines),

except for the κ_{ARM}/IRM_{100} ratio. The tephra layers were excluded in the downcore magnetic profiles, in order to highlight the environmental implications of the magnetic properties results.

Unit 7 (122.4–106 m depth).

The basal unit is dominantly composed of regularly laminated sets of rhythmic light/dark fine laminae of facies 15. The diatom assemblages are dominated by freshwater taxa (*Stephanodiscus niagarae* and *S. oregonicus*), which in this unit reach their highest concentration. At the lower part of the sequence, there is a 1.5 m thick deposit of the carbonate-rich silt of facies 18. There are also 13 beds of micritic mud (F19). Peaks in Ca/Ti ratio correlate to these micritic beds and the facies 18 sediments, but in general this ratio in facies 15 sediments is rather low. This behavior is also observed in the Mn/Fe ratio. Fe/Ti relation in this unit shows the highest values in the whole sequence, and they are particularly high in the carbonate rich sediments of facies 18 and 19.

Concentration-dependent parameters χ , χ_{ARM} , SIRM and HIRM₃₀₀ show a similar pattern. Variable but high values below 118 m depth are found in the basal sediments of facies 15 and in the carbonate-rich sediments of facies 18 (χ 0.04–0.2 10^{-6} m³/kg, χ_{ARM} 0.2–2 10^{-6} m³/kg, SIRM 0.5–5 mAm²/kg and HIRM₃₀₀ 0.02–0.6 mAm²/kg). The lowest values are present where the micritic mud beds of facies 19 are more frequent, while some maxima are associated with volcaniclastic deposits. The κ_{ARM} /IRM₁₀₀ presents its highest values below 118 m depth (~0.007 m/A), and remains

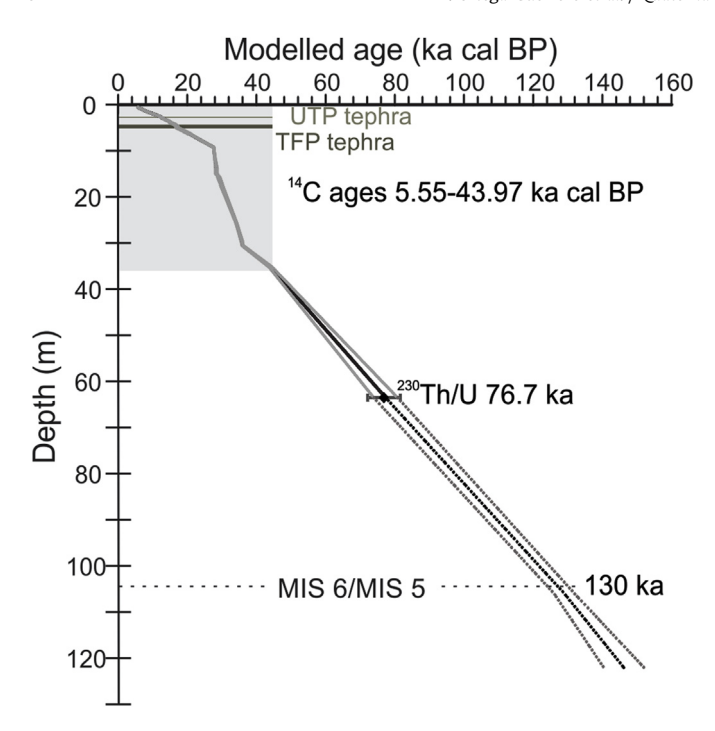


Fig. 3. Chronology of the Lake Chalco sedimentary sequence. The P-sequence model generated with calibrated ¹⁴C values (shaded area) and ages of the Upper Toluca Pumice (UTP), Tutti Frutti Pumice (TFP), the ²³⁰Th/U age and the age boundary of MIS 6/MIS 5 (Table 1 Supplementary Material).

mostly constant upwards the record. The κ fd% is very variable (as in all the record), with average values 3–6%. The upper section of this

unit (above 118 m depth), presents some of the lowest concentration-dependent parameters values in all the record; χ is mostly lower than 0.08 10^{-6} m³/kg, χ_{ARM} ranges from 0.05 to 1.9 10^{-6} m³/kg, SIRM varies from 0.3 to 4.7 mAm²/kg and HIRM₃₀₀ from 0.01 to 0.5 mAm²/kg. This unit presents some of the lowest coercivity values of the entire record. HIRM₃₀₀, S₃₀₀ and Bcr present similar variations, the higher coercivity is found in the sediments of facies 18 (HIRM₃₀₀ ~ 0.5 mAm²/kg, S₃₀₀ ~ 0.75, Bcr ~ 120 mT), the lowest in the sections with higher abundance of facies 19 sediments (HIRM₃₀₀ 0.001–0.08, S₃₀₀ 0.8–0.9, Bcr 52–80), while the facies 15 sediments present intermediate values. The kfd% shows large variations (1–10%); it peaks where concentration is high (ca. 114 m depth), and in general is lower between 113 and 106 m depth (average 1–6%).

Unit 6 (106-57.5 m depth).

A sharp change is recorded in most parameters at 106 m depth, with the onset of sediments of facies 7. Calcareous biogenic components (Chara sp., ostracods, calcareous particles and some Phacotus loricas) are common in the entire unit. Higher Ca/Ti ratio is also a common characteristic of this unit. Diatoms decrease their concentration in relation to the previous unit, and are dominated by alkaliphilous and halophilous species such as Cyclotella meneghiniana or Campylodiscus clypeus, and large struvite crystals are found, as well as occasional calcite and gypsum. This pattern is interrupted at around 100 m depth, where the laminated sediments of facies 14 are dominated by freshwater Stephanodiscus spp. diatom taxa and diatom concentration slightly increases. This variation is also observed in the decrease of Ca/Ti ratio. Upwards. there are several changes in facies association and calcareous clavey silt massive sediments of facies 10 (up to 83.3 m depth), and facies 11 and 5 become dominant towards the top of the unit. Along the unit, the sandy facies 6 are frequent. Sediments of facies 6, 7, 10, 11

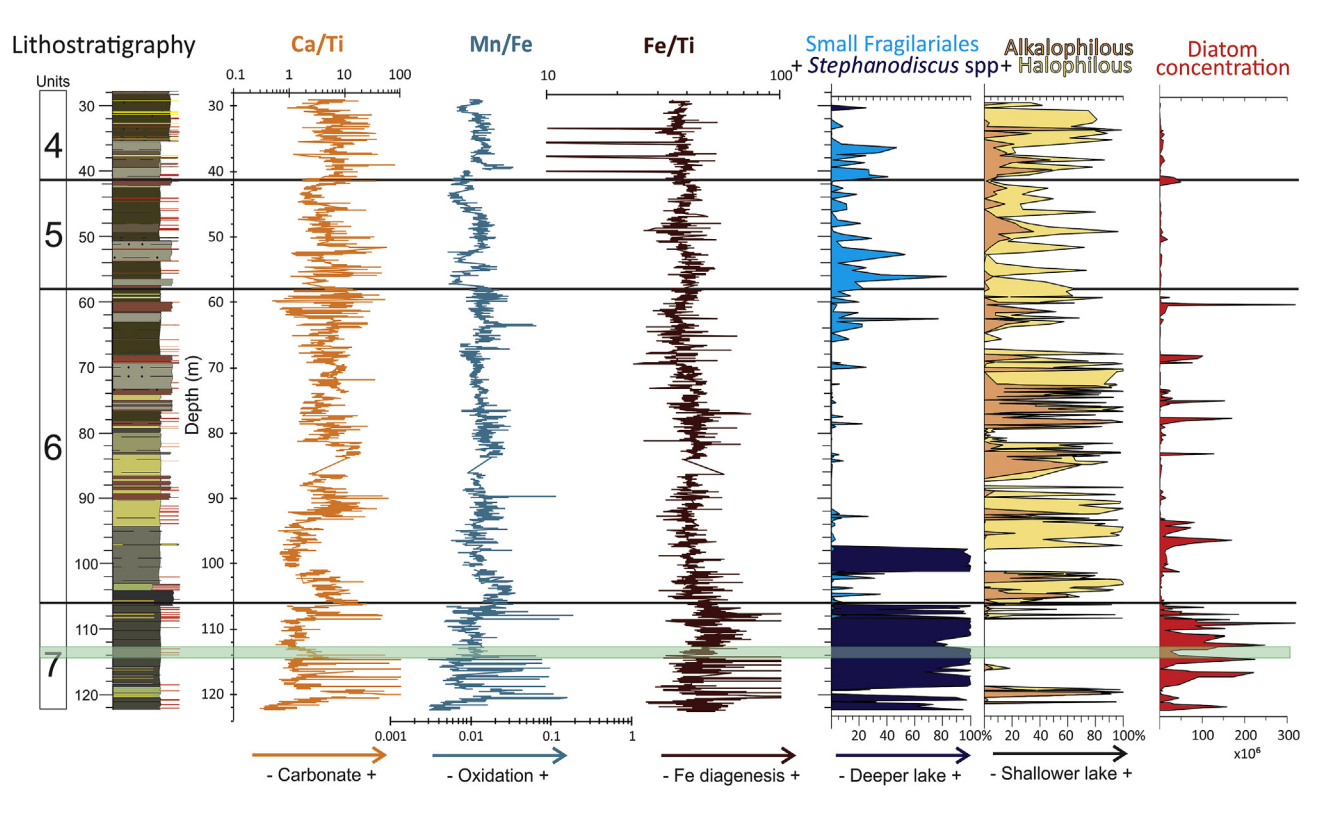


Fig. 4. Lithostratigraphy of master sequence of CHA08 cores and geochemical data. Ca/Ti is an indicator of authigenic carbonate in the lake. Mn/Fe ratio is an oxidation indicator. Fe/Ti is a proxy of diagenetic Fe enrichment. Freshwater diatom taxa (small Fragilariales and *Stephanodiscus* spp.), and alkaliphilous and halophilous taxa show nearly an opposite distribution. Diatom concentration is expressed in 10⁶ valves/gram of dry sediment.

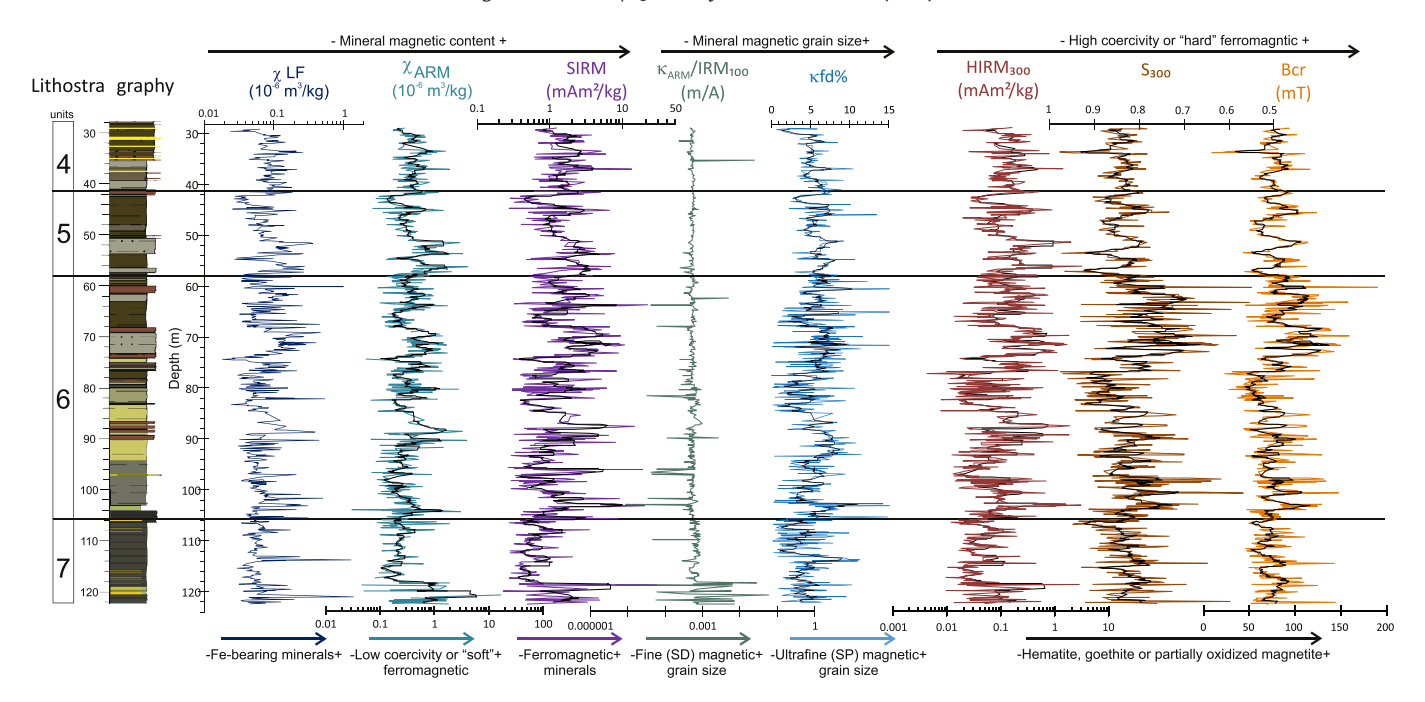


Fig. 5. Down-core profiles of magnetic parameters of CHA08 Lake Chalco cores. Concentration-dependent parameters χ , χ_{ARM} , SIRM and HIRM₃₀₀, grain size-dependent ratio $\kappa_{ARM}/100$ IRM₁₀₀ and κ fd%, and magnetic mineralogy indicators HIRM₃₀₀, S₃₀₀ and Bcr. The black lines are 5-point running average.

and 18 present relatively high Ca/Ti. Mn/Fe ratios are relatively high in the lower part of this unit, in facies 7 and 18. Fe/Ti remains relatively constant along this unit.

Most of the magnetic parameters show their highest amplitude fluctuations along this unit. χ , χ_{ARM} , SIRM, κ fd%, HIRM $_{300}$ and S_{300} have their highest values in the lower part of the unit, in facies 18 and 14, and in the sandy sediments of facies 6 and 11 (χ 0.06–4.5, χ_{ARM} 0.2–1.5, SIRM 1–20, κ fd% 3–15%, HIRM $_{300}$ 0.1–1.8); and the lowest in the facies 10, 12 and 5. The coercivity parameters also show a strong correlation among them and with the sedimentary facies. As in the case of the concentration parameters, the highest coercivities are found in sediments of facies 18, and in the sandy sediments of facies 11, 7 and 6 (S_{300} 0.55–0.7, Bcr 70–160); while the lowest coercivities are present in the facies 10, 12 and 5.

Unit 5 (57.5-41.1 m depth).

This unit is comprised mainly by the sediments of facies 5 and 11, and occasionally by the facies 9 and 6. Below 50.6 m depth the sediments are mostly massive with mottled intervals, and above this depth are bedded at centimetric to decimetric scale. Calcareous organic and inorganic components are common. Diatoms are a minor constituent, small Fragilariales, which have their highest abundances in this unit, alternate with alkaliphilous and halophilous diatoms. Where facies 11 and 6 sediments are present, Ca/Ti (~10–50) and Mn/Fe (~0.01–0.02) are relatively higher. Fe/Ti shows minor fluctuations between 30 and 50.

Magnetic mineral concentration proxies show their highest values in the unit at its bottom, where the sandy sediments of facies 11 are more abundant (χ 0.1–0.35, χ_{ARM} 0.4–4, SIRM 1–8, HIRM $_{300}$ 0.06–3). Concentration parameters values decrease upward, above 50 m depth, in facies 5 sediments (χ ~ 0.04, χ_{ARM} 0.08, SIRM ~ 0.3, HIRM $_{300}$ ~ 0.03). Several higher values are associated to clastic-rich sediments of facies 5 around 45 m depth. Coercivity variations are similar to those found in the concentration parameters. Coercivity is higher in facies 11 sediments (HIRM $_{300}$ ~ 3, S_{300} ~ 0.78, Bcr ~ 120), and diminishes in the upper part of the unit, except around 45 m depth where concentration values increase. $\kappa fd\%$ varies in average 4–8%.

Unit 4 (41.1–29 m depth).

This unit is composed mainly by facies 5 and 11 and in lower proportion by facies 6, 9 and 17. Sediments of facies 5 have higher sand-size clastic content than in lower beds of the same facies. Sediments are mostly massive, centimetric and decimetric beds are visible at some intervals. In the lower section (41.1—35.5 m depth) the same alternation between the small Fragilariales and the alkaliphilous and halophilous diatoms is observed. In the upper part of this unit, the higher frequency of ostracod hash beds of facies 17 is characteristic. *Chara* sp. is also a main biogenic carbonate producer present in this part. Diatoms are occasionally partly dissolved and dominated by alkaliphilous and halophilous species as *Cyclotella meneghiniana*, *Nitzschia frustulum*, *Navicula elkab* and *Chaetoceros* spp. Ca/Ti ratio shows high values, mostly 3—10, with peaks (30) in facies 6 and 17. Mn/Fe and Fe/Ti present rather uniform values, similar to those of the lower part of unit 5.

Magnetic mineral concentration and coercivity are relatively high along the unit ($\chi \sim 0.06-0.25$, χ_{ARM} 0.2–2, and SIRM 0.7–6; HIRM₃₀₀ 0.06–0.5, S₃₀₀ 0.78–0.88, Bcr 60–120). Slightly lower concentration values are found in facies 9 sediments around 38 m depth, in facies 5 sediments at ca. 33 m depth, and in the topmost sediments of this unit. Coercivity fluctuations are also analogous to the observed in concentration, it is lower in facies 9 and 5, and relatively higher in the rest of the sediments. κ fd% has no clear relationship with the sedimentary facies, it varies between 4 and 7% in average in most of this unit, and decreases at the top of the sequence.

4.2. Magnetic properties of sedimentary facies

4.2.1. Temperature-dependence of susceptibility $(\kappa-T)$

The thermomagnetic analyses show in all cases an increase in magnetic susceptibility after heating. The cooling curves (Fig. 6, blue lines), reflect the formation of new magnetic minerals during the heating (Fig. 6, red lines). The first derivative of the heating and cooling curves helps to identify the range of temperatures at which the main inflection of these curves occurred. The subtle inflection

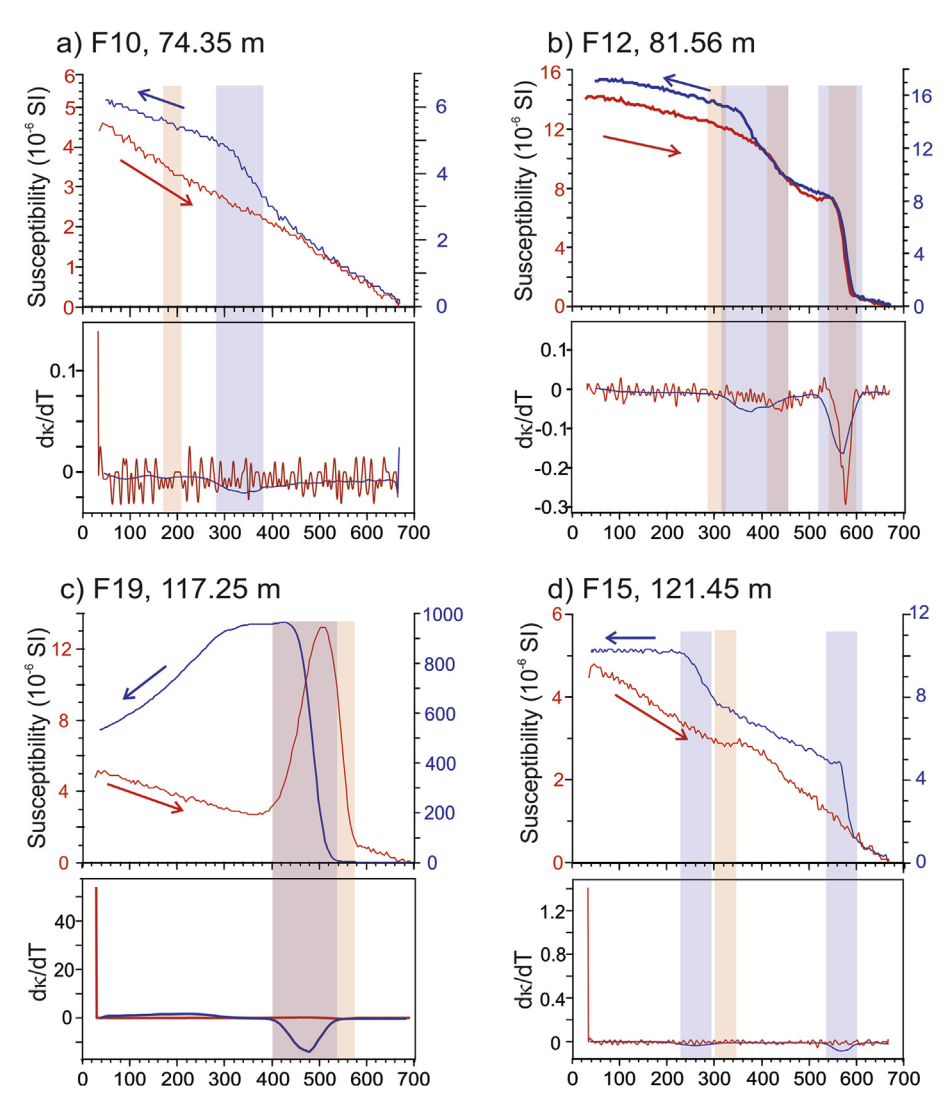


Fig. 6. Thermomagnetic curves (κ vs. temperature, or κ -T) for selected samples of different facies (Fx) and depths (m) from Lake Chalco. First derivative curve (d κ /dT), show the main inflections of the heating (red rectangles) and cooling (blue rectangles) curves. Note the different scales of magnetic susceptibility (κ) for the heating curves (red) and the cooling curves (blue). (For interpretation of the references to color in this figure legend, the reader is referred to the Web version of this article.)

found near 200 °C in several samples corresponds to the Curie temperature (TC) of Ti-rich titanomagnetite (Fig. 6a). The TC range from 400 to 500 °C correspond to Ti-poor titanomagnetite, and the TC near 580 °C correspond to almost pure magnetite (Fig. 6b). The samples containing Ti-magnetite/magnetite content show the most reversible curves of all samples (Fig. 6a and b). In these samples, the cooling curves indicate the persistence of these more thermally stable mineral phases after heating.

Some samples exhibit an inflection around 300 °C in the heating curves and a large increase in κ in the cooling curves, which may be due to the inversion of Ti-maghemite (Fig. 6b and d) (Özdemir and O'Reilly, 1982; Liu et al., 2005). Carbonate rich sediments have a singular upward peak between 400 and 580 °C during warming (Fig. 6c), a behavior typical of the transformation of siderite into magnetite (Housen et al., 1996; Isambert et al., 2003; Vázquez-Castro et al., 2008). In this sample (Fig. 6c), the 100-fold increase in κ after heating is remarkable.

All samples measured show a decrease in κ during heating in temperatures higher than 600 °C, which indicate the presence of Ti-hematite or hematite. These mineral phases may correspond to detrital minerals, or to the transformation of titanomaghemite into

(Ti)-hematite, which in turn is transformed into magnetite during the cooling process.

4.2.2. Hysteresis properties

The Day diagram (Day et al., 1977; Dunlop, 2002a, 2002b), represents the distribution of coercivity and magnetization parameters. However, as the diagram has been shown to be ambiguous for the definition of domain states (Roberts et al., 2018), caution should be taken when using it as a guide to particle sizes. However, the distribution in the diagram can provide information about environmental processes (e.g. Rodelli et al., 2019). Samples fall on the PSD region, some of them close to the SD + SP mixture curve (Fig. 7a), but overall most of them plot away from the MD region. Selected samples from representative sedimentary facies in the Day diagram show the variability of hysteresis parameters within certain facies (Fig. 7b); for instance, sediments of facies F5 and F6 plot along the main extremes of all sample population. In general terms, the sediments with a higher content of sand-size grains plot in the PSD region towards the MD area, whereas those samples with finer-size particles plot close to the SD + SP mixing lines. Samples from tephra layers are displayed to emphasize the

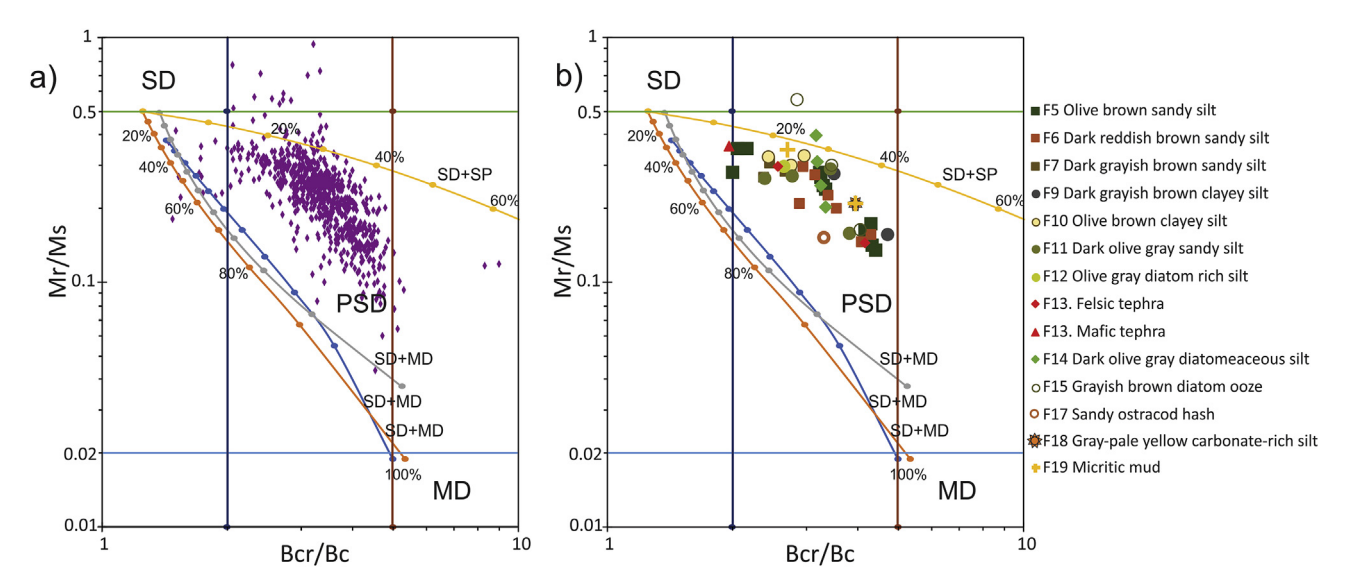


Fig. 7. Day plot (Mr/Ms versus Bcr/Bc) (Day et al., 1977). For the full data set (a), and selected samples with their sedimentary facies indicated (b). Theoretical mixing curves for magnetite mixtures are from Dunlop (2002a, 2002b).

range of coercivity and magnetization that relatively pristine grains may present.

4.2.3. Decomposition of IRM demagnetization curves

IRM demagnetization measurements were conducted on a collection of samples representative of the different sedimentary facies. The decomposition of the IRM curves allows to quantify the changes of the different fractions of magnetic mineralogy that contribute to the magnetic remanence, and therefore estimate the origin of the individual contributions and their variability over time. After unmixing of the IRM (Maxbauer et al., 2016b), most samples present 3 components, and a few are composed of 2 or 4 components (Fig. 1 Supplementary material, Supplementary material). A very low coercivity component of a mean coercivity (Bh) < 20 mT, with a dispersion parameter (DP) from 0.11 to 0.70, and an observed contribution (OC) from 3 to 30% of the total signal, is present in most samples. This is attributable to pedogenic or detrital soft magnetite (Egli, 2004; Lascu and Plank, 2013). Components of intermediate coercivity have [1] Bh 20-30 mT (DP 0.26-0.67; OC 6-23%), [2] 30-60 mT (DP 0.17-0.53; OC 7-97%), and [3] 60-100 mT (DP 0.20-0.45; OC 6–87%), respectively. The intermediate coercivity component [1] is typical of coarse detrital magnetite (Egli, 2003). The average DP observed for the intermediate coercivity [2] and [3] components are in general higher than values reported for low and high coercivity magnetofossils, 0.19 and 0.15, respectively (Egli, 2004), which indicates that the higher DP components correspond to nonbiogenic or altered magnetite crystals. Components of relatively higher coercivity have a Bh 100-125 mT (DP 0.35-0.48; OC 54-91%), 125-200 mT (DP 0.20-0.41; OC 46-78%), and >200 mT (DP 0.12-0.42; OC 1-7%). These higher Bh components can be interpreted as the contribution of oxidized magnetites/maghemites (van Velzen and Dekkers, 1999; Chen et al., 2005) or ultrafine hematite (Maxbauer et al., 2016c). Fig. 8 emphasizes the broad distribution of coercivities (Bh) and the large dispersion (DP) of modelled components in all the sedimentary facies of Lake Chalco. Only a constrained population of the mineral components have coercivities and narrow DP distribution to be considered as low coercivity magnetofossils, samples from facies 15 (118.19 and 121.47 m) and from facies 5 (54.84 and 66.5 m depth) (Table 2 Supplementary material). The relative percent contributions are summarized and shown according to the stratigraphic position in Fig. 5.

5. Discussion

5.1. Origin of magnetic minerals in cores CHA08 sediments

The results of our rock magnetic study show that the remanence is controlled mostly by low coercivity (Bh < 125 mT) ferromagnetic minerals, held by detrital partially oxidized Ti-magnetite/ maghemite according to the κ-T measurements. The detrital components have large DP, which implies a large grain size range. The range of coercivities found in the low coercivity (Bh < 125 mT) fraction may be due to different degrees of partial oxidation of Timagnetites. As (Ti)-magnetites are the most common detrital magnetic mineral in the volcanic rocks that outcrop in the basin, it is feasible that different degrees of partial oxidation of Timagnetites (via maghemitization) increased the range of coercivities of original minerals (e.g. van Velzen and Dekkers, 1999), and consequently increased the Bh and DP. The oxidation occurs at the borders of the grains inwards, while Fe²⁺ is oxidized and removed from the crystal (Maxbauer et al., 2016c). As the diffusion of Fe²⁺ progress, an oxidized (maghemitized) shell is formed around an unoxidized (magnetite) core (Ge et al., 2014). The lowtemperature oxidation of (Ti) magnetite to (Ti) maghemite can occur under oxic conditions in soils of the catchment area during weathering or diagenetic processes (e.g. van Velzen and Dekkers, 1999; Chen et al., 2005). The effect of the oxidation may be large in Ti-magnetites, increasing Mr/Ms and hardening the coercivity (Roberts et al., 2018), and this could cause the shift in the position for the most oxidized samples towards the top in the Day plot (Fig. 7).

In addition to Ti-magnetites/maghemites, the component of higher coercivity identified (Bh > 125 mT), suggests also the presence of hematite or goethite. The κ -T measurements also suggest the presence of hematite. In soils, goethite is favored in cool and moist conditions that only rarely experience prolonged intervals of aridity (e.g. Maxbauer et al., 2016c). By contrast, hematite is more abundant in subtropical or tropical soils with frequent episodes of prolonged dryness (e.g. Cornell and Schwertmann, 2003). The alteration of magnetite/maghemite or clay minerals, and the

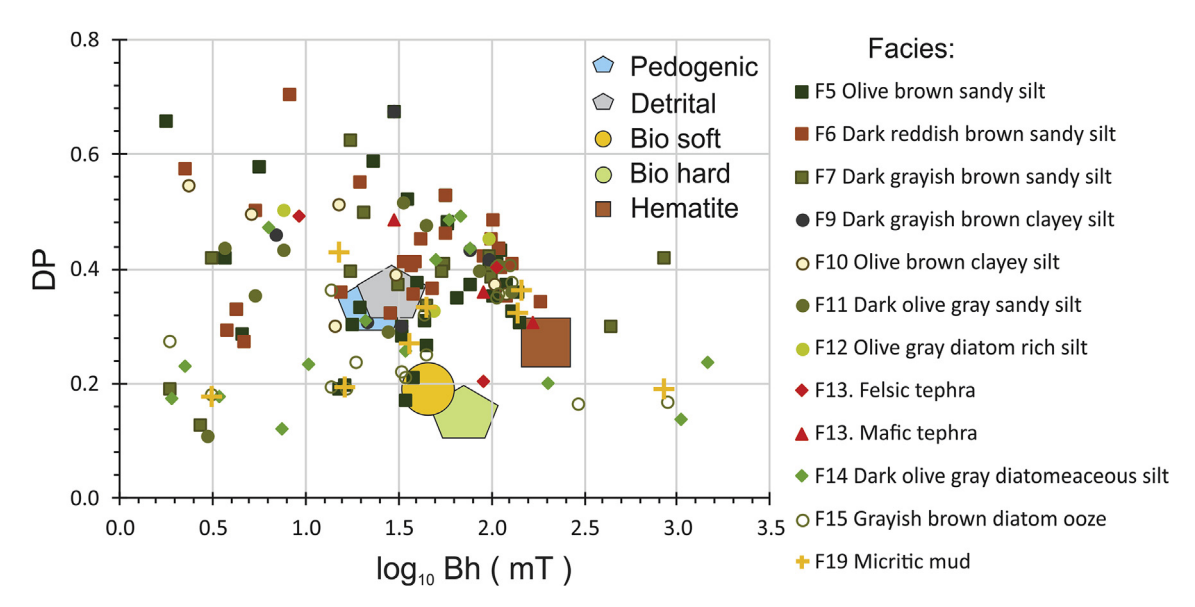


Fig. 8. Plot of the median coercivity (Bh) versus dispersion parameter (DP) for the magnetic components of sedimentary facies from Lake Chalco. The magnetic components were obtained from the unmixing of IRM demagnetization curves (Maxbauer et al., 2016b). Large symbols represent the end-members defined by Egli (2003, 2004) for pedogenic magnetite, detrital, low-coercivity magnetofossils (bio soft), high coercivity magnetofossils (bio hard) and hematite components.

dehydratation of goethite to hematite, can result in the formation of hematite (Maxbauer et al., 2016c). Hematite tends to have broad coercivity spectra that extends from low to high values, depending on the grain size; fine-grained hematite (16–100 nm) have coercivity values of ~10–200 mT, while large hematite crystals (0.1–2 mm) have even lower coercivity values of ~10–30 mT (Özdemir and Dunlop, 2014). Given the Bh values of the higher coercivity components in Lake Chalco sediments (>125 mT), they could reflect fine-grained hematite.

The relative abundance of the softest magnetic component (Bh < 20 mT), which can be attributable to pedogenic or detrital magnetite, was found in most of the analyzed samples. This soft component has no apparent clear relationship with the sedimentary facies or stratigraphic position, which make us think it can be both of origins. The presence of ultrafine SP minerals is suggested by $\kappa fd\% > 6\%$ in all units, in particular in unit 6 sediments (Fig. 5; Table 2 Supplementary Material), but they may have several possible origins and mineralogy. They can be either authigenic, detrital pedogenic, or magmatic minerals included in the detrital silicates, both magnetite or hematite. The formation of new minerals concerning redox processes is an aspect that is discussed later. The interplay between the magnetic minerals and past climatic fluctuations is discussed below.

5.2. Paleoenvironmental implications

The deposition of Unit 7 sediments occurred between ca. 146 to 130 ka (122.4—106 m depth), during the late part of Marine Isotopic Stage 6 (MIS 6, 191-130 ka BP), in cooler than present conditions as inferred from the presence of *Stephanodiscus* spp., a genus that today has a very restricted distribution in Mexico, but that was abundant in sedimentary sequences dating to the last glacial maximum in several records from the region (Bradbury, 2000; Metcalfe et al., 1991; Caballero et al., 2002; Valadez et al., 2005) (Fig. 9). The diatoms indicate also a fresh and relatively deep lake and thus relatively humid conditions (Avendaño-Villeda et al., 2018), a deep lake with anoxic bottom conditions was also favorable for the preservation of bands and laminae in the sediments. Diatom productivity is at its highest during this period. In the

sediments below 118 m depth (ca. 146-141.5 ka, facies 15 and 18), the locally high χ_{ARM} , κ_{ARM} /IRM and κ fd% values suggest the presence of SD and SP particles in some horizons, although it has been documented that interacting SP or PSD particles behave as SD (Muxworthy et al., 2003). In this section, the coercivity analysis shows that ~60% of the coercivity has a mean Bh of ~107 mT (Fig. 5), which is attributable to partially oxidized Ti-magnetite. However, there is also a magnetically soft component that contributes ~20% to the remanence, which may correspond to soft magnetosomes (Bh ~ 33 mT, DP ~ 0.2) (Egli, 2004; Lascu and Plank, 2013). The high values of χ and SIRM indicate higher ferrimagnetic (e.g. magnetite) mineral content, and higher Fe/Ti ratios point to an iron diagenetic enrichment, or lack of dissolution, which we suggest represents the magnetosomes. In agreement with the preserved laminae, this implies the existence of an oxic-anoxic interface, where the magnetotactic bacteria exist (Moskowitz et al., 2008). Therefore, the magnetic properties indicate that, in the lowest section of the record, higher sedimentary input by runoff under wetter environments coexisted with lower oxygen concentrations at the water/ sediment interface, conditions that temporally favored the formation and preservation of magnetotactic bacteria. Together, these processes resulted in the accumulation of detrital Ti-magnetite and fine-grained non-interacting SD equidimensional magnetite in the sediment (Egli, 2004; Lascu and Plank, 2013). At around 120 m depth (ca. 144 ka) the lake records a temporary change in environmental conditions. The facies 18 carbonate-rich sediments, the lower diatom concentration dominated by alkaliphilous and halophilous species and the higher values of Ca/Ti and Mn/Fe, indicate higher salinity, oxic bottom water conditions and thus suggest a lowering in lake level. The magnetic mineral parameters are highly variable in this section, but a moderate increase in coercivity is observed. Later on, a return to the previous higher lake level and anoxic bottom-water conditions is recorded.

In the upper part between 118 and 106 m depth (ca. 141.5–130 ka), where the laminae are best preserved, magnetic mineral concentration parameters decrease, large MD grains (low κ_{ARM} /IRM) were found, and coercivity analysis point to the lack of magnetosomes. This suggests a change in environmental conditions with respect to the previous stage. Siderite was observed in the

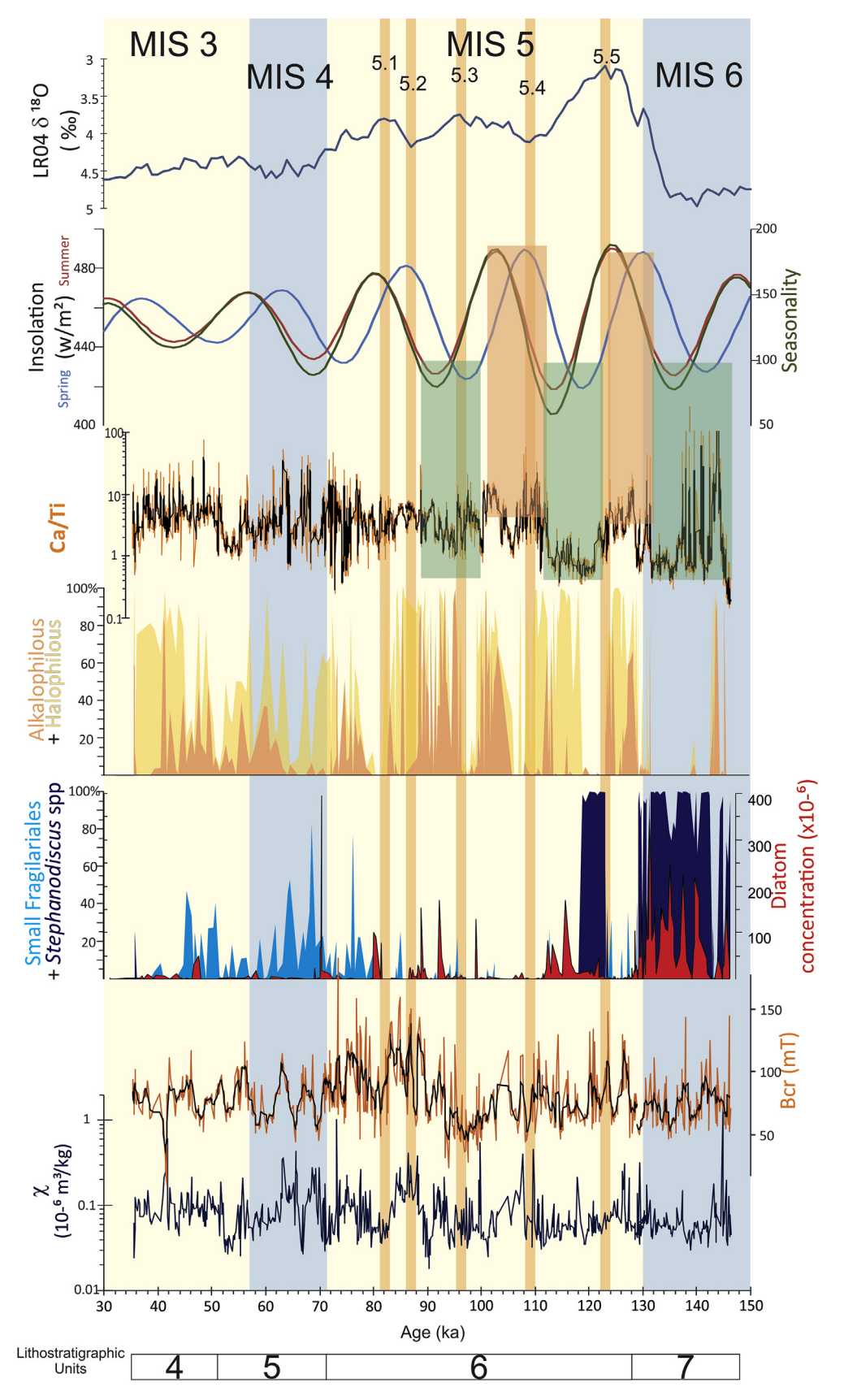


Fig. 9. Selected concentration (χ) and coercivity (Bcr) rock magnetic parameters, diatoms and carbonate content (Ca/Ti, 7-point-running average in black), plotted in time scale (ka) along the lithostratigraphic units, spring and summer insolation curves for 20°N obtained in the AnalySeries software (Paillard et al., 1996) according to the Laskar et al. (2004) solution, seasonality (summer-winter insolation), and the benthic δ^{18} 0 LR04 stack (Lisiecki and Raymo, 2005). Diatom record of deeper lake levels (Fragilariales and Stephanodiscus spp.) is plotted along diatom concentration. Blue shades indicate the cooler marine isotopic stages (MIS) 6 and 4, and pale yellow shades indicate the warmer MIS 5 and 3, and peaks of substages 5.5–5.1 (according to the Lisiecki and Raymo, 2005 nomenclature). Orange (green) shades point the occurrence of drier (less dry) conditions that correlate with maxima (minima) of spring and summer insolation. (For interpretation of the references to color in this figure legend, the reader is referred to the Web version of this article.)

carbonate rich sediments of this section, where Fe/Ti has some of the highest values in the record and Ca/Ti shows extreme peaks. κ -T measurements also pointed to the presence of siderite in the warming curve, which showed a characteristic peak above 400 °C as converted to magnetite (Housen et al., 1996; Vázquez-Castro et al., 2008). Under anoxic-non-sulfidic conditions, magnetite is unstable and may transform to siderite (FeCO₃) (Berner, 1981). The decrease in κ_{ARM} /IRM ratio and the lower κ fd% indicate a coarsening of magnetic minerals. These characteristics suggest the preferential dissolution of the finest Fe-oxide magnetic minerals under reducing-non-sulfidic conditions and the re-precipitation of the paramagnetic siderite. A deeper lake with periods of anoxic reducing conditions in the bottom may have prevented the preservation of magnetosome crystals, if they were formed at all. As the diatom assemblages in the micritic mud are mostly of freshwater habitats (Avendaño-Villeda et al., 2018), higher biological productivity must trigger an increase of pH and reduced the solubility of carbonates (Kelts and Hsü, 1978), promoting the precipitation of calcite and occasionally siderite in an anoxic bottom.

In this section, between 118 and 106 m depth, the most abundant magnetic component (~46-70%) is consistently harder (Bh 126-144 mT, DP 0.3-0.4) than in the lower part. This relatively hard phase may correspond to highly oxidized detrital Timagnetite/maghemite, hematite or goethite. We cannot make a definitive conclusion about the presence of goethite as our saturating fields (1 T) were too low to magnetize this mineral (Rochette et al., 2005). Hematite is less reactive in reducing environments than Ti-magnetites (Franke et al., 2007; Garming et al., 2007). whereas goethite is likely to have formed in the soils during the, in general, moist and cool climates inferred from diatoms. Regardless the composition of the Fe-oxides present, this implies that, in spite the existence of recurring anoxic conditions inferred for this section, the dissolution did not affect the totality of the Fe oxides and coarser particles were preserved (Jelinowska et al., 1997). The end of the MIS 6 (ca. 132-130 ka, 108.5–106 m depth) is characterized by oscillations in the diatom concentration and species, showing fluctuations between freshwater Fragilariales and halophilous and alkaliphilous species, which suggest relatively short-term alternations between drier and moister climate.

A change in environmental conditions is clearly observed in sedimentological, geochemical and magnetic characteristics and the diatom record after ca. 130 ka (106 m depth), at the beginning of the last interglacial (Fig. 9). Variations in magnetic parameters (mainly concentration and coercivity) are coeval with the change in facies deposition. The increase of the calcareous sedimentary components is reflected in increased Ca/Ti and in the alkaliphilous and halophilous diatoms. More oxic environment (>Mn/Fe) allowed the preservation of Fe oxides, and the diatom concentration records the lowest values (Fig. 5). The low concentration of diatoms may be a result to dilution by higher clastic components input (silt and clay), and lower diatom productivity during drier periods with higher lake salinity.

In units 6, 5 and 4, κ -T measurements and unmixed demagnetization of IRM curves indicate that the magnetic mineralogy is essentially the same, partially oxidized detrital Ti-magnetites are the main magnetic carriers and a smaller fraction (<21%) that may correspond to pedogenic magnetite (Bh < 20), and only the proportion among the fractions of different coercivity varies. Higher HIRM₃₀₀ also point to higher production of magnetically harder minerals (e.g maghemite, partially oxidized magnetite, hematite or goethite), especially in Unit 6 sediments (Fig. 5). The frequency dependence (κ fd%, 2–5%, mean 5%) found in units 6, 5 and 4 indicates the existence of ultrafine SP minerals, which may be associated with the pedogenic component. Hematite may also be present, but its origin is probably secondary as a result of low-

temperature oxidation of primary Ti-magnetite.

The changes in the concentration and in the coercivity spectra are related to the variability in the magnetic mineralogy. The carbonate-rich sediments tend to have higher coercivities and also higher abundance of alkaliphilous and halophilous diatoms (Fig. 9). The carbonate precipitation, the diatom species and the abundance of calcareous components as ostracods and *Chara*, indicates a saturated water column, a shallower lake, and in consequence environments with negative evaporation/precipitation balance. This suggests that higher oxidation of Ti-magnetites occurred during dry periods. The amplitude of fluctuations of rock magnetism parameters is higher in Unit 6, which is roughly coincident with MIS 5 (130-71 ka), but decrease in units 5 and 4, whose sediments were accumulated approximately during MIS 4 (71-57 ka) and the early part of MIS 3 (57-35 ka), respectively.

During the global warmer temperatures of MIS 5 occur the highest amplitude variability of the analyzed proxies. The maximum in coercivity parameters (e.g. Bcr) and alkaliphilous and halophilous diatoms, along with calcareous sedimentary components and higher carbonate content (>Ca/Ti), indicate that higher evaporation and prolonged dry periods during warmer conditions alternated with less dry and probably temperate environments (Fig. 9). At the early MIS 5 (ca. 130-123 ka, 106-101 m depth), the increases in sedimentary input ($>\chi$), in coercivity (Bcr), in the geochemical ratios Ca/Ti and Mn/Fe, and the dominance of alkaliphilous and halophilous diatoms, mark the onset of dry conditions. This interval was followed by a return of a phase (ca. 123 to 118 ka, 101-97 m depth), after the peak of the last interglacial period (5.5, 123 ka), of conditions similar than those present during MIS 6. as indicated by the diatom freshwater species and the lowering of Ca/Ti. Later, during the MIS 5 (ca. 118 to 80 ka, 97-66 m depth), Stephanodiscus spp. disappears, diatom concentration decreases and alkaliphilous and halophilous diatom species become dominant, with only the sporadic presence of small Fragilariales. During this period, higher carbonate content (>Ca/Ti) and higher coercivity is found, whose maximum are at around ca. 102 and 86 ka (84 and 71 m, respectively). Decreases in the carbonate content (<Ca/Ti) occur when halophilous diatoms are dominant (as at ca. 116, 106, 93 and 84 ka). Together, all these characteristics indicate that dry conditions prevailed during most of the MIS 5. Under this environment the higher oxidation of Fe-bearing minerals occurred, and Chalco was a shallow lake of alkaline-saline waters as result of high evaporation, whose conditions were unfavorable for the flowering and preservation of diatoms. The end of MIS 5 (80-71 ka, 66-61 m depth) is characterized by swings between small Fragilariales freshwater diatoms and alkaliphilous - halophilous diatom species. The peaks of Fragilariales are coeval with lower Ca/Ti and coercivity, which indicate a change towards less dry climatic conditions.

Through the globally colder MIS 4 (71-57 ka, 58.2-46.3 m depth), freshwater and saline-alkaline diatoms oscillate as during the end of MIS 5, although the Fragilariales show higher abundance than during the previous stage; however, diatom concentration remains low. Minimum [maximum] in carbonate content (Ca/Ti) correlate to peaks of Fragilariales [alkaliphilous + halophilous] ca. 69, 65 and 59 ka [ca. 63 and 67.5 ka], which are nearly coincident with decreases [increases] in Bcr. The characteristics of MIS 4 suggest that periods of higher evaporation, dry conditions and a saline-alkaline environment in the lake alternated with reduced evaporation, less dry conditions and freshwater lake periods, the later probably associated to colder climate. Even though Fragilariales diatoms point to a moderate amelioration of dry conditions, the climate was mostly dry. This period (69-59 ka) has been associated with high fire activity and drought frequency in the Chalco basin (Torres Rodríguez et al., 2015, 2018).

Similar characteristics to those that occurred during MIS 4 are

recorded during the analyzed period of MIS 3 (57–35 ka, 46.3–29 m depth). At the early MIS 3 (ca. 55 to 51 ka, 44.5–41 m depth) lower carbonate content (<Ca/Ti) coincide with higher content of halophilous diatoms and low concentrations of Fragilariales. After ca. 51 ka, variations between freshwater and alkalinesaline lake alternate until ca. 39 ka, thereafter halophilous diatoms become dominant. Peaks in drier conditions occur around ca. 55 and 38 ka. These drier conditions are also documented in the pollen record of Lake Chalco (Torres-Rodríguez et al., 2018). Our data suggest that even if dry conditions persisted in the globally cooler MIS 4 and in the less cool early MIS 3, they were of lesser intensity than in MIS 5.

In contrast to MIS 6, in which high values of magnetic susceptibility (χ) and magnetic concentration-dependent parameters are associated with higher runoff under wetter conditions and the preservation of magnetotactic bacteria, high χ is coeval with several of the inferred drier conditions during MIS 5-3 (except around ca. 102, 90, 74 and 68 ka). In several paleoclimatic records, χ is interpreted as a proxy of increased rainfall (e.g. Hodell et al., 2008). However, the Lake Chalco data show that mineral magnetic concentration is also associated to sedimentary input by surficial runoff under drier conditions, probably associated with an unprotected catchment surface or littoral by the lack of vegetation cover and, hence, higher sediment availability.

Modern precipitation in central Mexico occurs substantially during the summer, when tropical convective activity as in the northward migration of Intertropical Convergence Zone, the easterly waves or tropical cyclones, constitutes the elements that result in precipitation (Magaña et al., 2003). The highest temperatures are reached in spring, just before the summer rainy season starts. A relative minimum in precipitation in the middle of the rainy season is observed over southern Mexico, related to fluctuations in sea surface temperature over tropical eastern Pacific, in turn modulated by the effects of incoming insolation (Magaña et al., 2003). Previous studies have shown that Lake Chalco display a pattern of orbital scale climatic variability that follows evaporation-insolation and seasonality (highest summer and lowest winter insolation) over the last ca. 40 ka (Lozano García et al., 2015; Caballero et al., 2019). In those studies, the highest carbonate content and salinity are associated to maxima in summer insolation and seasonality. In contrast, lower salinities and lowest temperatures during the last glacial maximum (LGM) correspond with minima in spring and summer insolation. In the longer record of Lake Chalco presented in this work, these relationships are recognized for some intervals. The cold and humid conditions recorded at the end of MIS 6 (except during a short period around ca. 144 ka), correlate with low spring insolation (Fig. 9). As discussed before, the freshwater diatom species found in the micritic mud suggest that carbonate content is related to a reduced the solubility of carbonates rather than a carbonate precipitation controlled by evaporative concentration. Minima of spring and summer insolation and lower evaporation (<Ca/Ti) are also observed at ca. 122-112 ka, and less clearly at ca. 100-88 ka. At the onset of MIS 5, maxima in spring and summer insolation and seasonality correlate with higher Ca/Ti, and this relationship is also observed between ca. 112-100 ka. For younger times, as seasonality decreases, the relation between carbonate content and insolation is not evident, which highlights that other climatic forcing than orbital scale precession induced insolation exerts higher control over climatic variability.

5.3. Regional patterns of climatic variability

In the pollen record of El Valle at the Central Panamanian lowlands, warmer than present conditions have been inferred between 126-118 ka, peaking around MIS 5.5 (123 ka), which are coeval to a decrease in precipitation with a propensity toward drought (Cárdenes-Sandí et al., 2019). The authors also found that during the following 118-97 ka period precipitation was similar or slightly wetter than modern. The Lake Chalco record shown here also suggests very dry conditions at ca. 127 ka, which prevail during most of the last interglacial, which is not consistent with the relatively humid conditions in Panamanian lowlands. Further south in the austral hemisphere, the Lake Titicaca records positive water balance and high lake levels coincide with glacial extent in adjacent Andes cordillera; conversely, a negative water balance and extremely low lake levels correspond to global warm periods, with the most saline (driest) periods occur during the last interglacial (D'Agostino et al., 2002; Fritz et al., 2007). The cold and wet conditions found in the Lake Titicaca record during global glacial stages are similar to those found in Lake Chalco during late MIS 6. On Iztaccíhuatl volcano (at the southeastern part of the basin of Mexico), the most extensive recorded glacial advance (Nexcolango) occurred during MIS 6 at around 190 ka and reached ca. 3000 m a.s.l. (Vázquez-Selem and Heine, 2011). This altitude is nearly coincident with the upper limit of the Sierra Nevada piedmont. This suggests that the MIS 6 is recorded in central Mexico as a particular cold and humid glacial period, more intense than MIS 2. In the Lake Petén Itzá sedimentary sequence in lowland Guatemala, moist conditions are recorded from ca. 85 to 48 ka (Hodell et al., 2008), which are contemporary to the drier/wetter oscillations found in Lake Chalco during the late MIS 5, the MIS 4 and the early MIS 3. In the Lake Peten Itzá record, a shift towards drier conditions and the onset of dry-wet alternations were found in sediments after ca. 48 ka, which, in Lake Chalco, coincide with the return to dry

The major wet-cold/dry-warm changes found along the Titicaca and Chalco lacustrine records imply a strong influence of the eccentricity. This cold/wet relationship is not found during the Last Glacial Maximum (ca. 26.5–19 ka BP) in the Lake Chalco diatom record, where the coldest phases are coincident with low precipitation (Caballero et al., 2019), suggesting that the MIS 6 and the LGM are not perfect analogues. Our data highlights the influence on local and regional climate of shorter scale climatic variability (orbital and millennial).

Within the uncertainties and limits of our time-scale model, the 150-32 ka Lake Chalco record, precession-induced insolation apparently influenced the precipitation along the last glacial.

6. Conclusions

The multiproxy investigation in the sediments of Lake Chalco presented here provides one of the longest records of the paleoclimatic conditions in the North American tropics.

Our results indicate that coeval variations of magnetic properties with geochemical data and diatom assemblages reflect the major climatic changes that occurred between ca. 35 and 150 ka BP, since the transition from the glacial MIS 6 to the last interglacial MIS 5.5, and through the last glacial (MIS 5.4 to the initial part of MIS 3).

The mineral magnetic assemblage of lacustrine sediments is controlled by relatively low coercivity (Bh < 125 mT) ferromagnetic minerals, likely held by detrital partially oxidized Ti-magnetite/ maghemite. Weathering or diagenetic processes have altered in different degrees the detrital low coercivity mineral population by partial oxidation of Ti-magnetites (via maghemitization). The nearly opposite distribution of freshwater diatom taxa (small Fragilariales and *Stephanodiscus* spp.), and alkaliphilous and halophilous taxa enabled us to infer changes from deep to shallow lake levels, the later also recognized by higher carbonate content.

Humid and cooler than present conditions occurred during the

MIS 6 record, with deeper lake levels after ca. 141.5 ka. The main environmental change is observed in all analyzed parameters after ca. 130 ka, at the beginning of the last interglacial when lake level dropped and climate became drier. A return to moister and cooler conditions is recorded after the peak of the last interglacial period (5.5, 123 ka). Large amplitude changes between 130-74 ka are roughly coincident with the MIS 5. The higher magnetic concentration and higher coercivity, along with larger carbonate content and the predominance of alkaliphilous and halophilous diatoms suggest that higher oxidation of Ti-magnetites occurred during dry periods. The amplitude of these changes decreases in MIS 4 (71-57 ka) and the early part of MIS 3 (57-35 ka).

Within the limitations of our age model, we observe that the variations in the analyzed parameters follow orbital-scale climatic oscillations at the early part of our Lake Chalco record. Low summer and spring insolation and lower seasonality inhibited evaporation and favored high lake levels during the MIS 6. During the global warmer MIS 5 correlation between maxima in spring and summer insolation and drier conditions is found around ca. 130-122 and 112-100 ka.

The Lake Chalco data shown in this work also suggest very dry conditions by ca. 127 ka, and their persistence during most of the last glacial, which contrast with the relatively humid conditions in Panamanian lowlands. The cold and wet conditions found in the Lake Titicaca record during global glacial stages are similar to those found in Lake Chalco during the glacial MIS 6.

This cold/wet relationship is not found during the Last Glacial Maximum (ca. 26.5–19 ka BP) in the Lake Chalco diatom record, where the coldest phases are coincident with drier conditions (Caballero et al., 2019), suggesting that the MIS 6 and the LGM are not perfect analogues.

These major wet-cold/dry-warm changes are related to the global glacial/interglacial transition from MIS 6 to the last interglacial MIS 5.5, which implies a strong influence of eccentricity. However, in the last glacial between 144-88 ka, precession-induced insolation changes controlled precipitation.

Declaration of competing interest

The authors declare that they have no conflicts of interests to this work.

CRediT authorship contribution statement

Beatriz Ortega-Guerrero: Data curation, Investigation, Writing - original draft. Diana Avendaño: Formal analysis, Writing - original draft. Margarita Caballero: Data curation, Investigation, Writing - original draft. Socorro Lozano-García: Writing - original draft. Erik T. Brown: Formal analysis. Alejandro Rodríguez: Formal analysis. Bernardo García: Formal analysis. Hermenegildo Barceinas: Formal analysis. Ana María Soler: Formal analysis. Albán Albarrán: Formal analysis.

Acknowledgements

This project was possible by the financial funding of projects UNAM-PAPIIT (Universidad Nacional Autónoma de México) IV100215, IN105918, IN103819and CONACyT 130963; and the support of the Ejido Tulyehualco authorities that facilitated the access to the drilling site. We thank the staff of National Lacustrine Facility (LacCore, University of Minnesota), D. Schnurrenberger, A. Myrbo, A. Noren and K. Brady for assistance with initial core description. XRF core scanning were performed at the Large Lakes Observatory, University of Minnesota-Duluth. Hysteresis parameters were measured at the Institute for Rock Magnetism, University

of Minnesota. The IRM is made possible through the Instrumentation and Facilities program of the National Science Foundation, Earth Science Division and by funding from the University of Minnesota. We thank M. Jackson and all the IRM staff for their invaluable assistance. We also thank Dr. Susana Sosa for technical support during field and laboratory work. C.L. Romero and S. García collaborated in the elaboration of the figures. The authors thank to two anonymous reviewers whose comments and suggestions improved the manuscript.

Appendix A. Supplementary data

Supplementary data to this article can be found online at https://doi.org/10.1016/j.quascirev.2020.106163.

References

- Arce, J.L., Layer, P.W., Lassiter, J.C., Benowitz, J.A., Macías, J.L., Ramírez-Espinosa, J., 2013. 40Ar/39Ar dating, geochemistry, and isotopic analyses of the quaternary Chichinautzin volcanic field, south of Mexico City: implications for timing, eruption rate, and distribution of volcanism. Bull. Volcanol. 75 (12), 774.
- Aufgebauer, A., Panagiatopoulos, K., Wagner, B., Schaebitz, F., Viehberg, F.A., Vogel, H., Zanchetta, G., Sulpizio, R., Leng, M.J., Damaschke, M., 2012. Climate and environmental change over the last 17 ka recorded in sediments from Lake Prespa (Albania/F.Y.R. of Macedonia/Greece). Quat. Int. 274, 122–135. https://doi.org/10.1016/jquaint.2012.02.015.
- Avendaño-Villeda, D.A., Caballero, M., Ortega-Guerrero, B., Lozano-García, S., Brown, E., 2018. Condiciones ambientales a finales del Estadio Isotópico 6 (El 6: > 130000 años) en el centro de México: caracterización de una sección de sedimentos laminados proveniente del Lago de Chalco. Rev. Mex. Ciencias Geol. 3582, 168—178.
- Bradbury, J.P., 2000. Limnologic history of Lago de Pátzcuaro, Michoacán, México for the past 48,000 years: impacts of climate and man. Palaeogeogr. Palaeoclimatol. Palaeoecol. 163, 69–95.
- Berner, R.A., 1981. A new geochemical classification of sedimentary environments. J. Sediment. Petrol. 51, 359–365.
- Borruel-Abadía, V., Gómez-Paccard, M., Larrasoaña, J.C., Rico, M., Valero-Garcés, B., Moreno, A., Jambrina-Enríquez, M., Soto, R., 2015. Late Pleistocene to Holocene palaeoenvironmental variability in the north-west Spanish mountains: insights from a source-to-sink environmental magnetic study of Lake Sanabria. J. Quat. Sci. 30 (3), 222–234. https://doi.org/10.1002/jqs.2773.
- Bronk-Ramsey, C., 2008. Deposition models for chronological records. Quat. Sci. Rev. 27, 42–60.
- Bronk-Ramsey, C., 2009. Bayesian analysis of radiocarbon dates. Radiocarbon 51 (1), 337–360.
- Caballero, M., Lozano, S., Ortega, B., Urrutia, J., Macias, J.L., 1999. Environmental characteristics of lake Tecocomulco, northern basin of Mexico, for the last 50,000 years. J. Paleolimnol. 22 (4), 399–411.
- Caballero, M., Ortega, B., Valadez, F., Metcalfe, S., Macias, J.L., Sugiera, Y., 2002. Sta. Cruz Atizapan: a 22-ka lake level record and climatic implications for the late Holocene human occupation in the Upper Lerma Basin, central Mexico. Palaeogeogr. Palaeoclimatol. Palaeoecol. 186, 217–235.
- Caballero, M., Lozano-García, S., Ortega-Guerrero, B., Correa-Metrio, A., 2019. Quantitative estimates of orbital and millenial scale climatic variability in central Mexico during the las 40,000 years. Journal of Quaternayr Science Reviews 205, 62–75. 0.1016/j.quascirev.2018.12.002 (SCI=4.334).
- Cárdenes-Sandí, G.M., Shadik, C.R., Correa-Metrio, A., Gosling, W.D., Cheddadi, R., Bush, M.B., 2019. Central American climate and microrefugia: a view from the last interglacial. Quat. Sci. Rev. 205, 224–233.
- Chen, T., Xu, H., Xie, Q., Chen, J., Ji, J., Lu, H., 2005. Characteristics and genesis of maghemite in Chinese loess and paleosols: mechanism for magnetic susceptibility enhancement in paleosols. Earth Planet. Sci. Lett. 240, 790–802.
- Cornell, R., Schwertmann, U., 2003. The Iron Oxides. Structure, Properties, Reactions, Occurrences and Uses. In: 2nd, Completely Revised and Extended Edition. Wiley-VCH, p. 664.
- D'Agostino, K., Seltzer, G.O., Baker, P.A., Fritz, S.C., Dunbar, R.B., 2002. Late-Quaternary lowstands of Lake Titicaca: evidence from high-resolution seismic data. Palaeogeogr. Palaeoclimatol. Palaeoecol. 179, 97–111.
- Day, R., Fuller, M., Schmidt, V., 1977. Hysteresis properties of titanomagnetites: grain-size and compositional dependence. Phys. Earth Planet. Inter. 13, 260–266.
- Dunlop, D., 2002a. Theory and application of the Day plot (Mrs/Ms versus Hcr/Hc) 1. Theoretical curves and tests using titanomagnetite data. J. Geophys. Res. 107 https://doi.org/10.1029/2001JB000486.
- Dunlop, D., 2002b. Theory and application of the Day plot (Mrs/Ms versus Hcr/Hc) 2. Application to data for rocks, sediments, and soils. J. Geophys. Res. 107 https://doi.org/10.1029/2001JB000487.
- Egli, R., 2003. Analysis of the field dependence of remanent magnetization curves. J. Geophys. Res., Solid Earth 108 (B2), 2081. https://doi.org/10.1029/2002JB002023.

- Egli, R., 2004. Characterization of individual rock magnetic components by analysis of remanence curves. 3. Bacterial magnetite and natural processes in lakes. Phys. Chem. Earth 29, 869–884.
- Evans, M.E., Heller, F., 2003. Environmental Magnetism. Principles and Applications of Environmagnetics. Academic Press, San Diego.
- Ferrari, L., Orozco-Esquivel, T., Manea, V., Manea, M., 2012. The dynamic history of the Trans-Mexican Volcanic Belt and the Mexico subduction zone. Tectonophysics 522, 122–149.
- Franke, C., Pennock, G.M., Drury, M.R., Engelmann, R., Lattard, D., Garming, J.F.L., von Dobeneck, T., Dekkers, M.J., 2007. Identification of magnetic Fe-Ti oxides in marine sediments by electron backscatter diffraction in scanning electron microscopy. Geophys. J. Int. 170, 545–555.
- Fritz, S., Baker, P.A., Seltzer, G.O., Ballantyne, A., Tapia, P., Cheng, H., Edwards, L.R., 2007. Quaternary glaciation and hydrologic variation in the South American tropics as reconstructed from the Lake Titicaca drilling project. Quat. Res. 68, 410–420.
- Garming, J.F.L., von Dobeneck, T., Franke, C., Bleil, U., 2007. Low-temperature partial magnetic self-reversal in marine sediments by magnetostatic interaction of titanomagnetite and titanohematite intergrowths. Geophys. J. Int. 170, 1067–1075
- Ge, K., Williams, W., Liu, Q., Yu, Y., 2014. Effects of the core-shell structure on the magnetic properties of partially oxidized magnetite grains: experimental and micromagnetic investigations. Geochem. Geophys. Geosyst. 15, 2021–2038. https://doi.org/10.1002/2014.C005265.
- Groot, M.H.M., Bogotá, R.G., Lourens, L.J., Hooghiemstra, H., Vriend, M., Berrio, J.C., Tuenter, E., Van der Plicht, J., Van Geel, B., Ziegler, M., others, 2011. Ultra-high resolution pollen record from the northern Andes reveals rapid shifts in montane climates within the last two glacial cycle. Clim. Past 7, 299–316.
- Haberzettl, T., Corbella, H., Fey, M., Janssen, S., Lucke, A., Mayr, C., Ohlendorf, C., Schabitz, F., Schleser, G., Wille, M., Wulf, S., Zolitschka, B., 2007. Lateglacial and Holocene wet—dry cycles in southern patagonia: chronology, sedimentology and geochemistry of a lacustrine record from Laguna Potrok Aike, Argentina. Holocene 17, 297—310. https://doi.org/10.1177/0959683607076437.
- Hodell, D.A., Anselmetti, F.S., Ariztegui, D., Brenner, M., Curtis, J.H., Gilli, A., Grzesik, D.A., Guilderson, T.J., Müller, A.D., Bush, M., Correa-Metrio, A., Escobar, J., Kutterolf, S., 2008. An 85-ka record of climate change in lowland Central America. Quat. Sci. Rev. 27 (11–12), 1152–1165.
- Housen, B.A., Banerjee, S.K., Moskowitz, B.M., 1996. Low-temperature magnetic properties of siderite in marine sediments. Geophys. Res. Lett. 23, 2843–2846.
- Isambert, A., Valet, J.P., Gloter, A., Guyot, F., 2003. Stable Mn-magnetite derived from Mn-siderite by heating in air. J. Geophys. Res.: Solid Earth 108 (B6).
- Israde-Alcántara, I., Velázquez-Durán, R., Lozano-García, M.S., Domínguez-Vázquez, G., Garduño-Monroy, V.H., 2010. Evolución Paleolimnológica del Lago Cuitzeo, Michoacán durante el Pleistoceno-Holoceno. Bol. Soc. Geol. Mex. 62 (3), 345–357.
- Jelinowska, A., Tucholka, P., Wieckowski, K., 1997. Magnetic properties of sediments in a Polish lake: evidence of a relation between the rock magnetic record and environmental changes in Late Pleistocene and Holocene sediments. Geophys. J. Int. 129, 727–736.
- Kelts, K., Hsü, K.J., 1978. Freshwater carbonate sedimentation. In: Lakes. Springer, New York, pp. 295–323.
- Lascu, I., Plank, C., 2013. A new dimension to sediment magnetism: charting the spatial variability of magnetic properties across lake basins. Glob. Planet. Chang. 110, 340–349.
- Laskar, J., Robutel, P., Joutel, F., Gastineau, M., Correia, A.C.M., 2004. A long-term numerical solution for the insolation quantities of the Earth. Astron. Astrophys. 428, 261–285.
- Lisiecki, L.E., Raymo, M.E., 2005. A Pliocene-Pleistocene stack of 57 globally distributed benthic δ18O records. Paleoceanography 20, PA1003.
- Lisiecki, L.E., Stern, J.V., 2016. Regional and global benthic d18O stacks for the last glacial cycle. Paleoceanography 31, 1368–1394.
- Liu, Q., Deng, C., Yu, Y., Torrent, J., Jackson, M.J., Banerjee, S.K., Zhu, R., 2005. Temperature dependence of magnetic susceptibility in an argon environment: implications for pedogenesis of Chinese loess/palaeosols. Geophys. J. Int. 161, 102–112.
- Lozano García, M.S., Ortega, B., Roy, P.D., Beramendi-Orosco, L., Caballero, M., 2015.

 Climatic variability in the northern sector of the American tropics since the latest MIS 3. Quat. Res. 84, 262–271. https://doi.org/10.1016/j.yqres.2015.07.002.
- Macías, J.L., Arce, J.L., García-Tenorio, F., Layer, P.W., Rueda, H., Reyes-Agustín, G., López-Pizaña, F., Avellán, D., 2012. Geology and geochronology of tlaloc, telapon, Iztaccíhuatl and Popocatépetl volcanoes, sierra Nevada, central Mexico. In: Aranda-Gómez, J.J., Tolson, G., Molina-Garza, R.S. (Eds.), The Southern Cordillera and beyond, vol. 25. Geological Society of America, pp. 163—193 (Field Guide).
- Magaña, V.O., Vázquez, J.L., Pérez, J.L., Pérez, J.B., 2003. Impact of El Niño precipitation in Mexico. Geofis. Int. 42 (3), 313–330.
- Maher, B.A., 2007. Environmental magnetism and climate change. Contemp. Phys. 48 (5), 247–274.
- Maxbauer, D.P., Feinberg, J.M., Fox, D.L., Clyde, W.C., 2016a. Magnetic minerals as recorders of weathering, diagenesis, and paleoclimate: a core—outcrop comparison of Paleocene—Eocene paleosols in the Bighorn Basin, WY, USA. Earth Planet. Sci. Lett. 452, 15—26.
- Maxbauer, D.P., Feinberg, J.M., Fox, D.L., 2016b. MAX UnMix: a web application for unmixing magnetic coercivity distributions. Comput. Geosci.-Uk 95, 140–145.
 Maxbauer, D.P., Feinberg, J.M., Fox, D.L., 2016c. Magnetic mineral assemblages in

- soils and paleosols as the basis for paleoprecipitation proxies: a review of magnetic methods and challenges. Earth Sci. Rev. 155, 28–48.
- Mays, J.L., Brenner, M., Curtis, J.H., Curtis, K.V., Hodell, D.A., Correa-Metrio, A., Escobar, J., Dutton, A.L., Zimmerman, A.R., Guilderson, T.P., 2017. Stable carbon isotopes (d13C) of total organic carbon and long-chain n-alkanes as proxies for climate and environmental change in a sediment core from Lake Petén-Itzá, Guatemala. J. Paleolimnol. 57, 307–319. https://doi.org/10.1007/s10933-017-9949-z.
- Metcalfe, S.E., Street-Perrott, F.A., Perrott, R.A., Harkness, D.D., 1991. Palaeolimnology of the Upper Lerma Basin, Central Mexico: a record of climatic change and anthropogenic disturbance since 11,600 yr BP. J. Paleolimnol. 5, 197–218.
- Metcalfe, S.E., Davies, S.J., Braisby, J.D., Leng, M.J., Newton, A.J., Terrett, N.L., ÓHara, S.L., 2007. Long and short-term change in the Pátzcuaro Basin, central Mexico. Palaeogeogr. Palaeoclimatol. Palaeoecol. 247, 272–295.
- Moskowitz, B.M., Bazylinski, D.A., Egli, R., Frankel, R.B., Edwards, K.J., 2008. Magnetic properties of marine magnetotactic bacteria in a seasonally stratified coastal pond (Salt Pond, MA, USA). Geophys. J. Int. 174, 75–92.
- Muxworthy, A., Williams, W., Virdee, D., 2003. Effect of magnetostatic interactions on the hysteresis parameters of single-domain and pseudo-single-domain grains. J. Geophys. Res. 108 (B11), 2517. https://doi.org/10.1029/2003JB002588.
- Nowaczyk, N.R., 2011. Dissolution of titanomagnetite and sulphidization in sediments from Lake Kinneret, Israel. Geophys. J. Int. 187, 34–44.
- Oliva-Urcia, B., Moreno, A., 2019. Discerning the major environmental processes that influence the magnetic properties in three northern Iberia mountain lakes. Catena 182, 104130. https://doi.org/10.1016/j.catena.2019.104130.
- Ortega, B., Caballero, C., Lozano, S., Israde, I., Vilaclara, G., 2002. 52 000 years of environmental history in Zacapu basin, Michoacan, Mexico: the magnetic record. Earth Planet. Sci. Lett. 202, 663—675.
- Ortega-Guerrero, B., Lozano-García, M.S., Herrera-Hernández, D., Caballero, M., Beramendi Orosco, L.E., Bernal, J.P., Torres-Rodríguez, E., Avendaño-Villeda, D., 2017. Lithostratigraphy and physical properties of lacustrine sediments of the last ca. 150 kyr from Chalco basin, central México. J. South Am. Earth Sci. 79, 507–524.
- Özdemir, Ö., Dunlop, D.J., 2014. Hysteresis and coercivity of hematite. J. Geophys. Res., Solid Earth 119, 2582–2594. https://doi.org/10.1002/2013JB010739.
- Özdemir, Ö., O'Reilly, W., 1982. An experimental study of the intensity and stability of thermoremanent magnetization acquired by synthetic monodomain titanomagnetite substituted by aluminium. Geophys. J. Int. 70 (1), 141–154.
- Paillard, D., Labeyrie, L., Yiou, P., 1996. Macintosh program performs time-series analysis. Eos Trans. AGU 77, 379.
- Reimer, P.J., Bard, E., Bayliss, A., Beck, J.W., Blackwell, P.G., Ramsey, C.B., Grootes, P.M., 2013. IntCal13 and Marine13 radiocarbon age calibration curves 0-50,000 years cal BP. Radiocarbon 55 (4), 1869—1887.
- Roberts, A.P., Tauxe, L., Heslop, D., Zhao, X., Jiang, Z., 2018. A critical appraisal of the "Day" diagram. J. Geophys. Res.: Solid Earth 123 (4), 2618–2644.
- Rochette, P., Mathé, P.-E., Esteban, L., Rakoto, H., Bouchez, J.-L., Liu, Q., Torrent, J., 2005. Non-saturation of the defect moment of goethite and fine-grained hematite up to 57 Teslas. Geophys. Res. Lett. 32, L22309 https://doi.org/10.1029/ 2005GI.024196.
- Rodelli, D., Jovane, L., Giorgioni, M., Rego, E.S., Cornaggia, F., Benites, M., et al., 2019. Diagenetic fate of biogenicsoft and hard magnetite in chemically stratified sedimentary environments of Mamanguá Ría, Brazil. J. Geophys. Res.: Solid Earth 124, 2313—2330, 10.1029/.
- Thouveny, N., Debeaulieu, J.L., Bonifay, E., Creer, K.M., Guiot, J., Icole, M., Johnsen, S., Jouzel, J., Reille, M., Williams, T., Williamson, D., 1994. Climate variations in Europe over the past 140 kyr deduced from rock magnetism. Nature 371,
- Torres Rodríguez, E., Lozano-García, S., Priyadarsi, R., Ortega, B., Beramendi, L., Correa Metrio, A., Caballero, M., 2015. Last Glacial droughts and fire regimes in the central Mexican highlands. J. Quat. Sci. 30 (1), 88–99.
- Torres-Rodríguez, E., Lozano-García, S., Caballero-Miranda, M., Ortega-Guerrero, B., Sosa-Nájera, S., Roy, P.D., 2018. Pollen and non-pollen palynomorphs of Lake Chalco as indicators of paleolimnological changes in high-elevation tropical central Mexico since MIS 5. J. Quat. Sci. 33 (8), 945–957.
- Valadez, F., Oliva, G., Vilaclara, G., Caballero, M., Rodriguez, D.C., 2005. On the presence of Stephanodiscus niagarae Ehrenberg in central Mexico. J. Paleolimnol. 34, 147–157. https://doi.org/10.1007/s10933-005-0810-4.
- Valero-Garcés, B., Stockhecke, M., Lozano-García, S., Ortega-Guerrero, B., Caballero, M., Fawcett, P., Werne, J.P., Brown, E., Sosa-Nájera, S., 2019. Stratigraphy and Sedimentology of the Upper Pleistocene Holocene Lake Chalco, México Basin. Limnogeology: Progress, Challenges and Opportunities: A Tribute to Beth Gierlowski-Kordesch. Editors: Michael R Rosen, Lisa Park-Boush, David B. Finkelstein, Sila Pla Pueyo. Springer (in press) (In revision).
- van Velzen, A.J., Dekkers, M.J., 1999. Low-temperature oxidation of magnetite in loess—paleosol sequences: a correction of rock magnetic parameters. Stud. Geophys. Geod. 43, 357–375.
- Vázquez-Castro, G., Ortega-Guerrero, B., Rodríguez, A., Caballero, M. y, Lozano-García, S., 2008. Mineralogía magnética como indicador de sequía en los sedimentos lacustres de los últimos ca. 2,600 años de Santa María del Oro, occidente de México. Rev. Mex. Ciencias Geol. 25 (1), 21–38.
- Vázquez-Selem, L., Heine, K., 2011. Late quaternary glaciation in Mexico. In: Quaternary Glaciations Extent and Chronology, Part III: South America, Asia, Africa, Australia, Antarctica 233-242. Elsevier, Amsterdam.